Magnetic Interactions Influencing Spectral Analysis and Quantitation in Nuclear Magnetic Resonance Spectroscopy

Harri Heikkinen

University of Helsinki
Faculty of Science
Department of Chemistry
A.I. Virtasen aukio 1 (P.O. Box 55)
FI-00014 University of Helsinki
Finland

Doctoral dissertation, to be presented for public discussion with the permission of the Faculty of Science of the University of Helsinki. In Auditorium PIII (Yliopistonkatu 3, Helsinki), on the 1st of November, 2019 at 12 o'clock.

ACADEMIC DISSERTATION

Supervisor

Professor Ilkka Kilpeläinen
Faculty of Science
Department of Chemistry
University of Helsinki, Finland

Reviewers

Professor Perttu Permi
Department of Chemistry
University Of Jyväskylä, Finland

Professor Emerita Tuula Pakkanen
Department of Chemistry
University of Eastern Finland, Finland

Opponent

Professor Ulla Gro Nielsen
Department of Physics, Chemistry and Pharmacy
University of Southern Denmark, Denmark

ISBN 978-951-51-5464-4 (paperback)
ISBN 978-951-51-5465-1 (PDF)
http://ethesis.helsinki.fi
Unigrafia Helsinki 2019

Abstract

There are many chemical analytical techniques available to probe molecular structures. Nuclear Magnetic Resonance (NMR) spectroscopy is an analytical spectroscopy technique that exploits strong external magnetic field and is capable of elucidating and quantifying molecular structures at the atomic level. NMR spectrum is typically measured from dissolved materials or directly from solid materials.

The influence of magnetic interactions in solution and solid-state define the information that is obtainable from the NMR spectrum. The molecular motion and mobility play a key role. The obtainable spectral resolution in solid-state is usually lower than in the liquid state due to the presence of anisotropic interactions, which are not averaged out like in solution state. In NMR this means that the spectra, which contain the structural information, can be visually very different. These phenomena, combined with the need to obtain quantitative information, need to be addressed with proper considerations when acquiring and interpreting NMR data. This thesis focuses on the impact of relevant magnetic interactions in NMR via selected chemical structure studies of materials such as lignin, Ziegler-Natta (ZN) and aluminosilicate catalysts and cellulose.

Tiivistelmä

On olemassa useita kemiallisia analytiikka tekniikoita, joilla voidaan tutkia molekyylien atomitason rakenteita. Ydinmagneettinen resonanssispektroskopia (NMR) on analyyttinen spektroskooppinen tekniikka, joka hyödyntää voimakasta ulkopuolista magneettikenttää ja jolla voi tunnistaa ja määrittää molekyylien atomitason rakenteita ja määriä. NMR-spektri mitataan tyypillisesti liuotetusta tutkittavasta yhdisteestä, liuoksesta tai vaihtoehtoisesti myös suoraan kiinteästä materiaalista.

Tutkittavien molekyylien magneettiset interaktiot määrittelevät pitkälti minkälaista informaatiota NMR-spektristä on mahdollista analysoida. Molekyylien liikkeellä on tässä asiassa suuri vaikutus. Saatavilla oleva NMR-spektrin resoluutio on tyypillisesti huonompi, jos NMR-spektri on mitattu kiinteästä materiaalista, kuin liuotetusta yhdisteestä. Tämä johtuu lähinnä anisotropiasta ja dipolaarisista kytkennöistä, joiden vaikutus liuostilan NMR-spektristä puuttuu. Käytännössä tämä näkyy siten, että liuostilan ja kiinteätilan NMR-spektrit voivat olla visuaalisesti hyvin erinäköisiä. Tämä spektrien fyysinen eroavaisuus yhdistettynä kvantitatiivisen atomitason tiedon määritykseen spektrin perusteella voi johtaa vääriin johtopäätöksiin. Tässä väitöskirjassa käsitellään magneettisten interaktioiden vaikutusta yleisesti NMR-spektroskopiassa ja NMR-rakennetutkimuksessa valikoitujen materiaalien (ligniini, Ziegler-Natta katalyytit, aluminosilikaatti katalyytit ja muokatut selluloosamolekyylit) avulla.

Acknowledgements

This work was conducted at VTT Technical Research Centre of Finland within the process chemistry division during 2008-2013 and at the University of Helsinki during 2015-2019. Funding was provided by TEKES – the Finnish funding agency for Technology and Innovation, the Academy of Finland, and the European Commission projects.

Obviously there are many persons to thank who have been involved during this process. Warm thanks goes to all my co-authors, colleagues and enablers who made this project possible. I would not have been able to do this without your help.

I owe the deepest gratitude to my supervisor Professor Ilkka Kilpeläinen who guided me through this process and introduced me to the world of NMR. I especially want to thank Dr. Andrew Root, an NMR entrepreneur, my friend, to have the persistence and patience to teach me solid-state NMR during this journey. I would also like to thank Dr. Hannu Maaheimo at the VTT Technical Research Centre for the support and advice, in NMR and life in general, Dr. Hideo Iwaï at the University of Helsinki for giving me an opportunity to learn new things in the world of biological NMR and in research in general, and Professor Paula Vanninen at VERIFIN for giving me an opportunity to join VERIFIN's group and to complete this project.

I wish to thank Professor Perttu Permi of University of Jyväskylä and Professor Emerita Tuula Pakkanen at the University of Eastern Finland for kindly reviewing this thesis.

I wish to thank my parents for everything. Especially my Dad - man who loved books. Here is one more to read up there. And finally, my heartfelt thanks to my spouse Anne and to my two lovely daughters, Lilja and Kaisla.

Helsinki, September 2019

Harri Heikkinen

List of publications

I **Harri Heikkinen**, Thomas Elder, Hannu Maaheimo, Stella Rovio, Jenni Rahikainen, Kristiina Kruus, Tarja Tamminen: Impact of steam explosion on the wheat straw lignin structure studied by solution-state nuclear magnetic resonance and density functional methods. (**2014**) *Journal of Agricultural and Food Chemistry 43(62),* 10437-10444. http://dx.doi.org/10.1021/jf504622j

II Juha Linnekoski, Martta Asikainen, **Harri Heikkinen**, Reetta Kaila, Jari Räsänen, Antero Laitinen, Ali Harlin: Production of p-cymene from crude sulphate turpentine with commercial zeolite catalyst using a continuous fixed bed reactor. (**2014**) *Organic Process Research & Development 18,* 1468-1475. http://dx.doi.org/10.1021/op500160f

III Sauli Vuoti, Elina Laatikainen, **Harri Heikkinen**, Leena-Sisko Johansson, Erkki Saharinen: Chemical modification of cellulosic fibers for better convertibility in packaging applications. (**2013**) *Carbohydrate Polymers 96,* 549-559. http://dx.doi.org/10.1016/j.cabpol.2012.07.053

IV Sauli Vuoti, Riku Talja, Leena-Sisko Johansson, **Harri Heikkinen**, Tekla Tammelin: Solvent impact on esterification and film formation ability of nanofibrillated cellulose. (**2013**) *Cellulose 20,* 2359-2370. http://dx.doi.org/10.1007/s10570-013-9983-6

V **Harri Heikkinen**, Tiina Liitiä, Ville Virkkunen, Timo Leinonen, Tuulamari Helaja, Peter Denifl: Solid state ^{13}C NMR characterization study on fourth generation Ziegler-Natta catalysts. (**2012**) *Solid State Nuclear Magnetic Resonance 43-44*, 36-41. https://doi.org/10.1016/j.ssnmr.2012.02.006

Author's contribution in the original publications

I HH planned the work and performed the NMR data analysis including data processing and analysis. HM and SR performed the experimental NMR work. HH drafted the manuscript, which was revised by all authors. All NMR experimental work was carried out at VTT Technical Research Centre. TE carried out all density functional method calculations and analysis. JR carried out sample preparation. TT and KK supervised the work.

II HH performed all experimental work related to NMR including the data interpretation and quantitative Brönstedt acid site calculations. HH wrote the NMR parts in the manuscript. All NMR experimental work was carried out at VTT Technical Research Centre. JL, MA, RK and JR conducted the practical laboratory catalysis reactions. AL and AH supervised the work.

III HH performed all NMR related experimental work including the data interpretation and degree of substitution (DS) calculations. HH wrote the NMR parts in the manuscript. All NMR experimental work was carried out at VTT Technical Research Centre. SV drafted the manuscript. SV, EL and ES planned and executed the synthesis of the cellulose samples. LSJ carried out the XRD related experimental work and analysis.

IV HH performed all NMR related experimental work including the data interpretation and degree of substitution (DS) calculations. HH wrote the NMR parts in the manuscript. All NMR experimental work was carried out at VTT Technical Research Centre. LSJ carried out the XRD related experimental work and analysis. SV and TT drafted the manuscript. RT planned and measured the barrier properties.

V HH performed all experimental work related to NMR, including spectra acquisition, data processing and analysis. HH and TLi drafted the manuscript, which was edited and approved by all authors. All NMR experimental work was carried out at VTT Technical Research Centre. VV, TLe and PD designed and executed the synthesis of the catalyst samples. TLi and TH also supervised the work.

List of abbreviations and acronyms

B_0	External magnetic field
B_1	Magnetic field by the nucleus
CP	Cross polarization
CSA	Chemical shift anisotropy
C_Q	Quadrupolar coupling
d_{IS}	Dipole-dipole coupling between I and S spins
δ_{iso}	Isotropic chemical shift
δ_{aniso}	Anisotropic chemical shift
DP	Direct polarization
eQ	Quadrupole moment
EFG	Electric field gradient
FT	Fourier transformation
FTIR	Fourier transformed infrared spectroscopy
FID	Free induction decay
γ	Gyromagnetic ratio
H-H	Hartman-Hahn matching
HSQC	Heteronuclear single quantum coherence
HMBC	Heteronuclear multiple bond correlation
$\hbar$	Reduced Planck constant
INEPT	Insensitive nuclei enhancement via polarization transfer
k_b	Boltzmann constant
MAS	Magic-angle spinning
μ_0	Vacuum permeability
NMR	Nuclear magnetic resonance
nOe	Nuclear Overhauser effect
r. f.	Radio frequency
SE	Steam explosion
S/N	Signal-to-noise
SSB	Spinning sideband
SSNMR	Solid-state NMR
T_1	Longitudinal relaxation time
T_2	Transverse relaxation time
T_R	Repetition time
T_{CH}	Contact time in H-H matching for ^1H-^{13}C spin pair
$T_{I\rho}$	T_1 relaxation in the rotating frame
η	Asymmetry parameter
ν_L	Larmor frequency
ZN	Ziegler-Natta

Table of Contents 1

1 Introduction

Nuclear magnetic resonance (NMR) spectroscopy is a technique that can probe the structure of a diverse range of materials at the atomic level. Since the discovery of NMR in the 1930s [1], and the subsequent development of Fourier Transformed NMR (FTNMR) [2] [3] and solid-state NMR (SSNMR) [4] [5] [6] [7] [8], it has been one of the main research tools for structure elucidation [9] [10] [11] [12] [13]. One of the reasons NMR has maintained its importance in the field of material research is because it can provide structural information in different material phases like solids or solutions. Due to this wide area of applicability, NMR has been used in both industry and academic research. In the field of biorefining, where new chemicals and high valued products are sought and made to replace fossil-based compounds, NMR can be especially very useful since the materials encompass a wide range of molecular sizes and may not be soluble in any media. Indeed, structural characterization in different material phases offers unique opportunities, but also challenges, since the mobility of the molecules differs substantially. In NMR, this means that the spectra, which contain the structural information, can be visually very different. This phenomenon, combined with the need to obtain quantitative information, need to be addressed with proper considerations when acquiring and interpreting NMR data. This thesis attempts to address these problems with respect to selected industrial applications that cover such materials as zeolite and Ziegler-Natta catalysts, lignin and cellulose. The theoretical aspects of NMR are kept at a minimal level and details concerning this can be found in the literature [14] [15] [32].

2 NMR spectroscopy

Although NMR spectroscopy can be used to study the vast majority of nuclei found in the periodic table (with spin $\geq 1/2$), usually the materials studied define the nuclei that are observed and commonly these include nuclei such as ^{1}H, ^{13}C, ^{15}N and ^{31}P. Similarly, as there exists a large variety of NMR experiments available and typically a selection of measurements are conducted, depending on the composition of the studied material and the information required from them.

2.1 Obtaining NMR spectra

NMR driven material characterization and structure elucidation is based on measuring NMR spectra and interpreting this data. NMR spectra are typically presented in ppm scale, and referenced to the resonance frequency of a reference compound. In this way the data obtained can be compared easily, and also universally, as it results in a field independent ppm value [14]. In principle, all NMR experiments can be described using simple blocks: preparation, evolution, mixing, and acquisition periods (Figure 1) [16] [10]. In the simplest one-dimensional (1D) NMR, only preparation and acquisition periods are included, whereas in two-dimensional (2D) NMR, all periods are included. In 2D NMR the evolution period is designed to allow certain, selected spins to evolve for a given length of time, and the mixing period is designed to transfer the magnetization between nuclei.

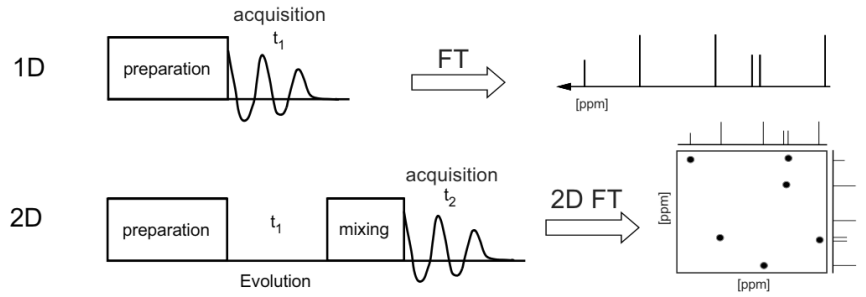

Figure 1 General schemes for 1D and 2D NMR experiments. NMR spectra is obtained by applying a Fourier transformation (FT) to the acquired data. In 2D NMR, an evolution period (t_1) is introduced to produce the second frequency dimension.

What makes NMR so interesting is the fact that there exist several different magnetic interactions, or perturbations, that are affecting the nuclei in different ways under the influence of strong magnetic fields. These magnetic interactions can be described using the following general Hamiltonian [35] [14]:

$$\mathcal{H} = \mathcal{H}_Z + \mathcal{H}_{RF} + \mathcal{H}_{CS} + \mathcal{H}_{DD} + \mathcal{H}_J + \mathcal{H}_Q + \mathcal{H}_{SR} \quad (2.1)$$

where $\mathcal{H}_Z$ is the main Zeeman interaction of nuclear spin and external magnetic field B_0,

$\mathcal{H}_{RF}$ is the coupling between the nuclear spin with the applied radio-frequency (RF) field, $\mathcal{H}_{CS}$ is the chemical shift (chapter 3.1), $\mathcal{H}_{DD}$ is the direct dipole − dipole interaction via magnetic moments (chapter 3.2), $\mathcal{H}_J$ is the indirect electron-coupled dipole-dipole interaction (chapter 3.3),), $\mathcal{H}_Q$ is the quadrupolar coupling associated to spin >1/2 nuclei (chapter 3.4) and $\mathcal{H}_{SR}$ is the spin-rotation interaction. All these interactions possess an isotropic and an anisotropic part [14] and contribute with varying magnitude to the layout of the measured NMR spectra. In general, in liquid state NMR only the isotropic parts of the Hamiltonian determine the form of the NMR spectra, while in solid-state NMR the anisotropic parts can also contribute. This usually results in higher resolution spectra in liquids than in solids.

In this study, the relevant perturbations are due to: a) chemical shift, b) dipolar coupling, c) indirect coupling, and d) quadrupolar coupling (for spins >1/2), which are briefly described. In liquids, we only retain the isotropic parts of a) and c). The isotropic values of b) and d) are zero (averaged out). In solids, all four interactions are non-zero and are contributing to the appearance of the NMR spectrum, usually by broadening the observed signal linewidth. In order to obtain quantitative data based on the NMR spectra in solution and in solid-state, these interactions and their consequence need to be considered (Chapter 3). Figure 2 illustrates those magnetic interactions, and other factors that are making a contribution to the final spectrum and are thus relevant from a quantitation point of view.

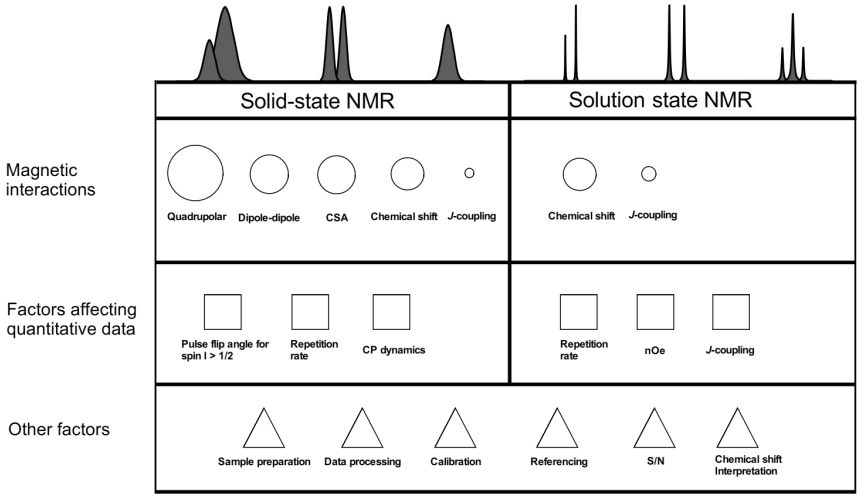

Figure 2 Relevant magnetic interactions and factors influencing spectral appearance and signal quantitation in solid-state and solution state NMR.

2.2 Obtaining quantitative NMR data

NMR spectroscopy is inherently a quantitative analytical method, provided certain precautions are taken. However, most of the NMR experiments, mainly multidimensional but also experiments with more sophisticated pulse schemes, usually result in non-quantitative spectral data due to several factors such as pulse imperfections, NMR hardware instabilities and the lack of uniform response of the sample [17] [18].

Quantitative NMR is a very attractive analytical choice as materials can be studied both in solution and in solid-state. The visual appearance of a solution state and solid-state NMR spectrum can be very different though, mainly due to the impact of different magnetic interactions causing severe line broadening depending on the molecular motion. This is mainly the case for the solid-state NMR spectrum, where all magnetic interactions are involved (Figure 2) and in turn typically causing the NMR FID signal to decay very fast and hence produce broad lines in the NMR spectra. This also has another consequence as the obtainable linewidth in solid-state NMR spectrum is sometimes insufficient to provide certain structural information as the signals are overlapping. Besides the magnetic interactions, there are several other factors, in addition to the already mentioned ones, affecting the quantitation in NMR spectroscopy. These factors include for instance sample

condition, sample preparation and data processing (Figure 2) and the reader in kindly asked to look in the literature for an in-depth analysis of these topics [10] [19].

In quantitative NMR, the signal areas in the NMR spectrum are proportional to the number of nuclei giving rise to it. To obtain quantitative data, the main issues to be addressed are utilization of the correct repetition time between pulses to allow the spins to relax back to thermal equilibrium and the consideration of the nuclear Overhauser effect (nOe). The importance of the *J*-coupling to adjacent nuclei is also important when magnetization is transferred via this interaction e.g. in 2D HSQC NMR experiments [21] [20].

As the T_1 relaxation processes follow the same mechanism in solid and solution-state [14], the relevance of using correct recycle times applies in both phases, although the T_1 values may vary significantly. If 90° excitation pulses are to be used, usually recycle times of 5 X T_1 are needed (recovery of magnetization >99%) [21]. For example, T_1 (^{13}C) values for certain crystalline polyethylenes in solid-state can be a few thousand seconds [22], which would make recycle times of the order of hours, which is really impractical from the instrument time point of view. In rigid systems where we are observing the less abundant spins S (e.g. ^{13}C) surrounded by more abundant spins I (e.g. ^{1}H) a cross-polarization (CP) pulse scheme can be used. In this case the magnetization is transferred from the I spins to the S spins and the repetition time is then defined by the I spin, which usually has usually much shorter T_1 values [23]. However, the data obtained using CP are no longer strictly quantitative *per se* as several factors are affecting its operation (CP dynamics).

Generally speaking, NMR experiments are always relative measures of signal intensities. This means that absolute population quantities need to be measured indirectly, using an internal or an external standard (referencing and calibration). Without the utilization of a standard sample, the NMR instrument related stabilities would also remain unknown. Related to this, a reasonable signal-to-noise (S/N) ratio in the NMR spectrum is needed in order to identify signals from the noise and to carry out reliable signal integration. As the NMR sensitivity is inherently weak [24], improvements in the NMR hardware, such as dynamic nuclear-polarization (DNP) [25] [26] or cryogenically cooled probe heads [27] [28] are improving the sensitivity and thereby enabling higher S/N to be obtained in shorter

periods of time.

2.3 Rationale of choosing correct NMR experiments

Due to the wide applicability of NMR spectroscopy, selecting the proper NMR experiment is important. Choosing the NMR experiment based on the studied materials is important for realizing the potential information that is obtainable from different experiments. For example, the 1D ^{1}H NMR spectrum in solution state is the easiest and usually also the quickest experiment to be measured from small organic molecules, whereas in solid-state NMR obtaining a high resolution ^{1}H NMR spectrum can be problematic. This is because the ^{1}H-^{1}H coupling network in solids broaden the signal linewidth even under MAS (Chapter 3.2), and usually only a few, broad signals are observed in 1D solid-state ^{1}H NMR spectra. There are exceptions though, like well-ordered zeolite materials where the proton density is low and the –OH moieties are sufficiently distant from each other so that the coupling network is weak. Thus, for zeolite and related materials, 1D ^{1}H solid-state NMR experiments can be measured to derive useful information using MAS (Chapter 4.2). Utilization of the 1D ^{1}H solid-state NMR experiment for cellulose based materials or other organic solids is of limited value unless special techniques are used, such as very fast MAS or multiple pulse NMR [29] [30], due to the strong ^{1}H-^{1}H coupling network and typically ^{13}C detection is preferred (Chapter 4.3).

The key difference between solution state and solid-state NMR lies in the molecular movement. In solution, only the isotropic chemical shift and *J*-couplings are observed (Figure 2), whereas in solid-state all interactions are present and contribute to the observed signal. Unfortunately, this usually broadens the observed signals in solid-state NMR spectrum but provides information that is not obtainable with solution state such as information regarding material crystallinity or metal coordination information (Chapter 4.4). All this kind of latter information is impossible to achieve using solution state NMR and sometimes it is important to measure the samples in solid-state even though the samples would be soluble to some media.

3 Magnetic interactions

Even though NMR theory follows the same principles in solid and liquid material phases, the relevance of the different magnetic interactions varies significantly. In the following paragraphs the relevant magnetic interactions affecting the appearance of the NMR spectrum are briefly introduced. The main interactions of interest here are the chemical shift anisotropy (CSA) and direct dipolar coupling – the usual sources of line broadening observed in solid-state NMR spectra (in the absence of quadrupolar nuclei).

3.1 Chemical shift

In a strong external magnetic field (B_0) the circulating electrons (spin ½) of an atom cause the local magnetic field experienced by the nucleus either to increase or decrease ($\mathcal{H}_{CS}$ in eq. 2.1) This effect, also known as *shielding* changes the observed Larmor frequency (ν_L) for individual nuclei and these changes in frequency are termed chemical shifts and give rise to different peak positions in the NMR spectrum for chemically different nuclei [31]. These peaks can be used to characterize the chemical structure of molecules.
The chemical shift is determined as a sum of isotropic and anisotropic contributions:

$$\delta = \delta_{iso} + 1/2\delta_{aniso}\,(3\cos^2\theta - 1 + \eta \sin^2\theta \cos 2\phi), \qquad (3.1)$$

where θ and ϕ define the orientation of the chemical shielding tensor with respect to the external magnetic field B_0 in a static frame [13]. In solution state, very rapid molecular tumbling averages out the anisotropic contribution and hence only the isotropic chemical shift remains and is observed in the spectrum. In a solid powder, all possible θ and ϕ orientations are possible and a broadened signal line shape is observed due to the CSA (Figure 3). The appearance of the broad line shape or ''powder spectrum'' depends on the symmetry of the local electron environment around the nuclei. Typically this is seen as a signal broadening caused by the individual molecule orientations with respect to B_0 forming the observed line width and shape (Figure 3). The chemical shift can be defined by three principal values δ_{11}, δ_{22}, δ_{33} (typically following positive high-frequency order $\delta_{11} > \delta_{22} > \delta_{33}$) in the principal axis of the nucleus [32] [132]. In solution state only the isotropic chemical shift is observed (i.e $\delta_{iso} = 1/3(\delta_{11} + \delta_{22} + \delta_{33})$). In order to attenuate the

effect of this anisotropic interaction in solids, a special technique called magic-angle spinning (MAS) can be used.

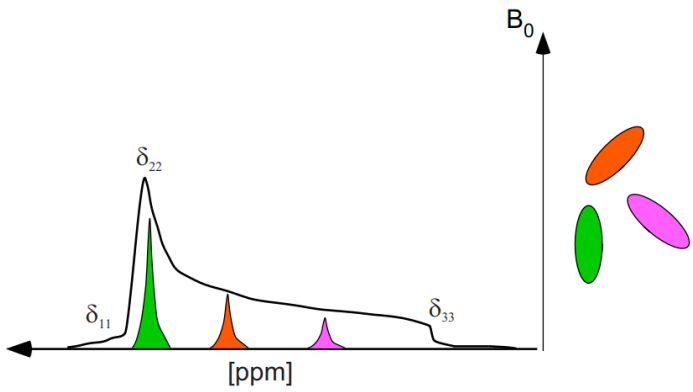

Figure 3 Typical appearance of a powder spectrum observed in solid-state NMR where the individual molecule orientations with respect to B_0 form the sum of the observed line shape in the presence of chemical shift anisotropy (CSA). The positions of the principal components (δ_{11}, δ_{22}, δ_{33}) are labelled and some individual crystallites are highlighted.

The MAS technique is used to remove anisotropic interactions and obtain high-resolution NMR spectra. Among the known magnetic interactions, chemical shift, heteronuclear dipolar coupling and first-order quadrupolar interactions all have a similar anisotropic time-averaged first-order angular dependence according to [32]:

$$\omega_{aniso} \propto (3\cos^2\theta - 1) = 1/2\,(3\cos^2\theta_R - 1)\,(3\cos^2\beta - 1) \qquad (3.2)$$

This equation can be fulfilled when the angle θ_R is set to 0.9553 rad (54.736°). This angle is thus termed the ''magic-angle'' because when the sample is spun continuously at this angle fast enough ($\omega_r > \omega_{aniso}$) the anisotropic interaction is removed and high-resolution NMR spectra can be obtained [33] [34]. Technically, this is achieved by mechanically spinning the sample placed inside a rotor at 54.7° with respect to the static field (Figure 4).

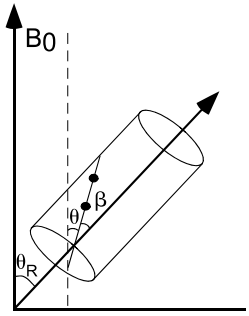

Figure 4 In the MAS technique, the sample is spun rapidly at 54.7° with respect to B_0 in order to remove anisotropic interactions, which cause signal line broadening in solid-state NMR spectra.

The size of the chemical shift anisotropy is proportional to the external magnetic field ($\delta_{aniso} \propto B_0$). In practice, it means that very high MAS rates are needed in high magnetic fields to remove CSA interactions. An interesting feature is observed in the spectrum of an inhomogeneous line shape (e.g. chemical shift anisotropy, 1st order quadrupolar interactions or isolated dipolar coupled spin pairs), when the MAS speed is less than the size of the anisotropic interaction, i.e. $\omega_r < \omega_{aniso}$: these inhomogeneous line shapes break up into spinning sidebands (Figure 5A). The spinning sidebands are located at an integer of the MAS rate from their corresponding isotropic chemical shifts. For a strongly multiple dipolar coupled system, where the signal line shape is more homogeneous, this is not observed at the same low MAS rates or may be significantly broadened. For these tightly coupled systems, very high MAS rates ($\omega_r > \omega_{aniso}$) are required to produce a spectrum where only the isotropic chemical shifts are present (Figure 5B). Therefore, MAS is a valuable technique which can effectively eliminate signal line broadening originating from both homo- and heteronuclear dipolar spin couplings, but the effectiveness depends on the nature of the dipolar coupling and the MAS rate (see chapter 3.2).

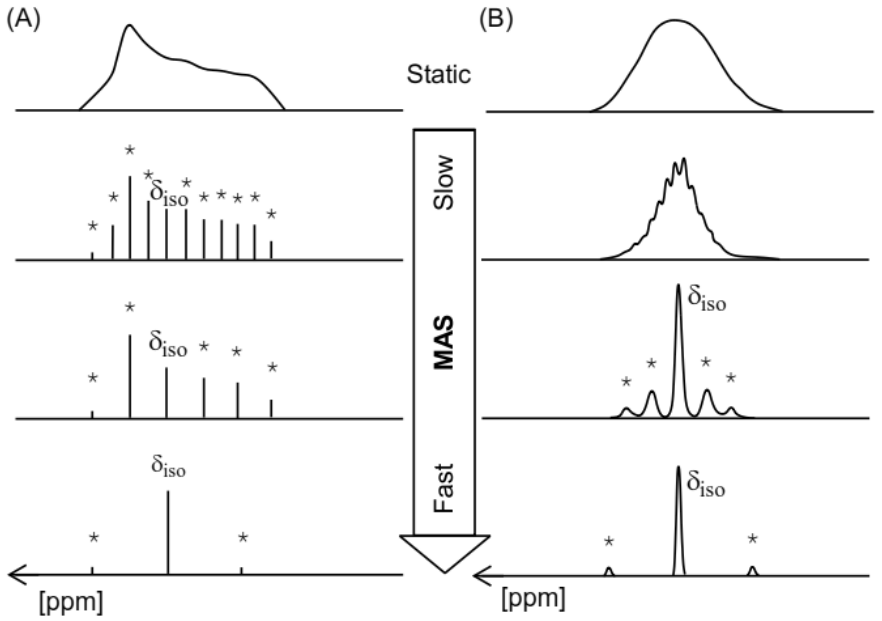

Figure 5 Schematic view of the effect of magic-angle spinning (MAS) on (A) inhomogeneously broadened line shape (e.g. CSA, isolated ^{13}C-^{1}H spin system), and (B) homogeneously broadened line shape (e.g. strongly coupled ^{1}H-^{1}H or ^{n}X-(^{1}H-^{1}H) systems). Spinning sidebands are marked with asterisks. Isotropic chemical shift (δ_{iso}) is highlighted to illustrate that its position (ppm) remains with different MAS rates.

Although MAS technique *per se* is not affecting the quantitation, integral areas of the spinning sidebands should be included with the integral area of the corresponding isotropic chemical shifts when measuring quantitative NMR. The spinning sidebands may also contain valuable structural information of the studied materials, which cannot be derived from the isotropic chemical shifts alone (Chapter 4.4).

3.2 Dipolar coupling

Nuclei can have a dipolar coupling (also known as dipole-dipole, direct coupling), which is mediated through space and does not require the presence of chemical bonds ($\mathcal{H}_{DD}$ in eq. 2.1). The size of this coupling exists at all distances but becomes large as the inter-nuclear distance decreases [14]. This coupling occurs as the magnetic nuclear spin produces a small magnetic field, which is felt by the second nucleus. As in the case for chemical shift, the

dipolar interaction (d_{IS}) has an orientation dependency and may be defined by [35] [36]:

$$d_{IS} = -\frac{\mu_0}{4\pi}\frac{\hbar\gamma_I\gamma_S}{r_{IS}^3}\left(\frac{3cos^2\theta-1}{2\pi}\right) \quad (3.3)$$

where μ_0 is the vacuum permeability, γ_I and γ_S are the gyromagnetic ratios of nuclei I and S, $\hbar$ is the reduced Planck constant, θ is the inter-nuclear vector with respect to the static magnetic field and r_{IS} is the distance between the two nuclei (I and S). Dipolar coupling can occur between both homonuclear (I-I) and heteronuclear (I-S) spins and may be either inter or intramolecular. The dipolar interaction is typically averaged to zero in solution state due to fast molecular tumbling. However, in the solid-state a range of dipolar couplings exist and lead to a powder spectrum where both homogeneous and inhomogeneous line shapes can be present, depending on the coupling system [14]. The MAS technique can be used to suppress the dipolar coupling, but its success depends heavily on the type of coupled spin system. For an isolated I-S spin system, moderately low MAS rates can be used to remove dipolar interaction as the couplings are assumed to be heterogeneous and no coupling in between this spin pair and other nuclei exists (Figure 6A). However, for so called homogeneous systems where I-I and I-S spins are coupled to the surrounding I spins (usually ^1H), low or moderate MAS rates are not able to average out the dipolar couplings. This is because the strongly coupled surrounding I spin network is modulated in time and results in spin diffusion. In order to remove dipolar couplings in such systems, the MAS rates should be higher than the I-I coupling system corresponding to the homogeneous line shape width ($\Delta\nu$) (Figure 6B).

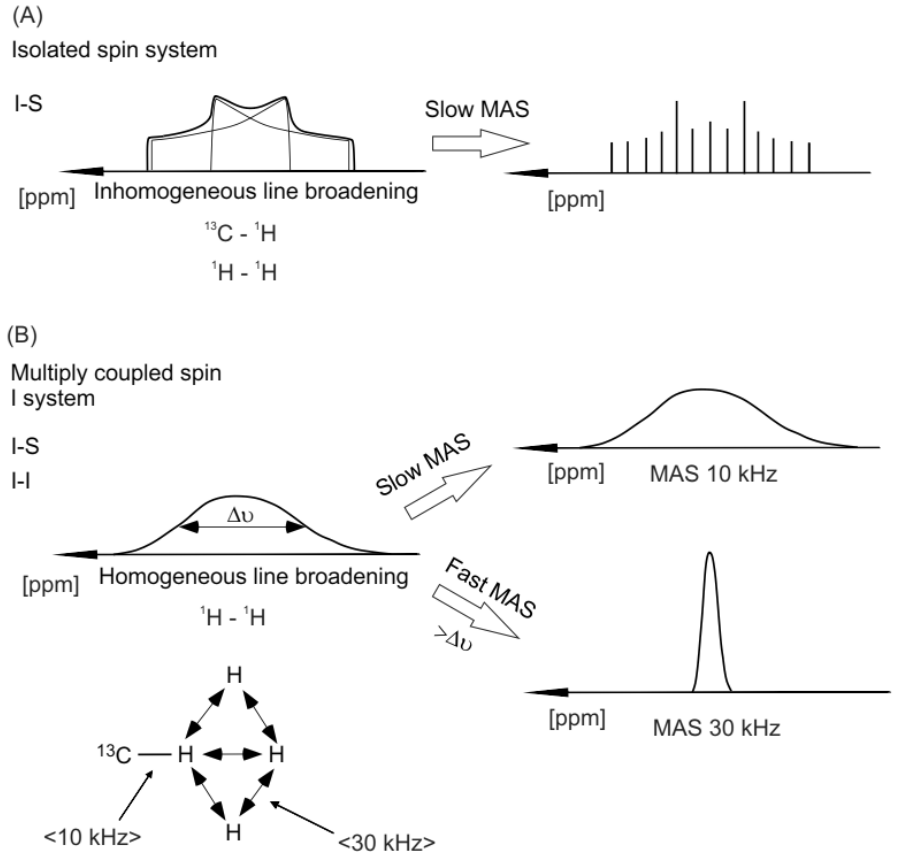

Figure 6 Schematic view of dipolar interactions and the effect of MAS to the spectrum for (A) isolated I-S spin pair, and (B) I-S and I-I spin pairs coupled to I system. For multiply coupled spin systems, very fast MAS rates are needed to remove dipolar couplings and to obtain narrower signal line shapes.

In solution state, the ^{1}H decoupling power (in experiments where it is used) does not need to be high as the very fast molecular tumbling averages out the direct dipolar couplings and only the scalar dipole-dipole couplings need to be removed [37] [10]. In solids, high-power decoupling schemes need to be utilized [38] [39] since the ^{13}C-^{1}H and ^{1}H-^{1}H dipolar couplings are not averaged out and the size of the dipolar-coupling network is usually in the range of tens of kHz in organic solids where all spins are coupled to each other.

The cross polarization (CP) technique [23] (combined with MAS and

high-power ^{1}H decoupling) is the most commonly measured solid-state NMR experiment to acquire spectra from organic solid samples. The CP technique is mainly employed to detect nuclei with low natural abundance, like ^{13}C (1.1%) [40] and ^{29}Si (4.7%) [41], yet the technique can also be utilized for any other nuclei, e.g ^{31}P (100%) [42]. In CP, the magnetization is transferred from an abundant I spin system (e.g. ^{1}H, ^{19}F) to the less abundant S spins (e.g. ^{13}C, ^{29}Si) in order to enhance their signal. This magnetization transfer provides two main benefits: first, signal amplitude is detected as an enhancement according to the gyromagnetic ratios γ_I/γ_S of the nuclei and secondly, the repetition time (T_R) between the pulse trains is dictated by the I spin spin-lattice (T_1) properties, which is usually much shorter than the T_1's of the S spins. A standard CP pulse sequence is illustrated in Figure 7. CP is started first by applying a 90º -pulse to the I spins, followed by an r. f. field applied simultaneously to I and S spins satisfying the Hartmann-Hahn (H-H) matching condition, i.e. $\gamma_I B_{1I}=\gamma_S B_{1S}$ [6]. S spin signal acquisition is usually carried out in the presence of high-power I spin decoupling [38] [39]. The CP experiment typically results in non-quantitative data as there are several factors affecting CP dynamics (nature of dipolar couplings (both I-I and I-S), distribution of nearby I spins, Hartmann-Hahn conditions, spin-diffusion, molecular motion, relaxation processes and MAS rate), which ultimately produce the observed signals in the spectrum [43]. Different methods are available to get more quantitative data when using CP [44] [45] [46].

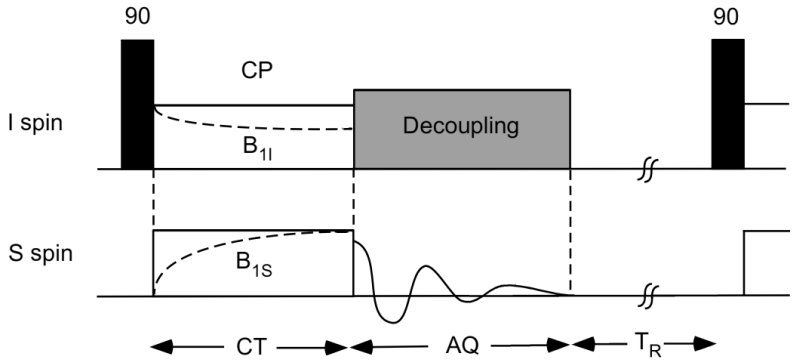

Figure 7 Schematic presentation of basic cross-polarization (CP) pulse sequence under Hartman-Hahn conditions $\gamma_I B_{1I}=\gamma_S B_{1S}$. Dashed lines in CP indicate $T_{1\rho}$ relaxation for I spin (B_{1I}) and CP buildup for S spin (B_{1S}) during CT. CT= contact time, AQ= acquisition time,

T_R=repetition time. Black rectangles indicate hard rectangular 90º ($\pi/2$) pulses. High-power I spin decoupling is shown in grey.

3.3 Indirect dipolar coupling

Another perturbation encountered in NMR spectroscopy that evolves between two spins is the indirect coupling (known as *J*-coupling or scalar coupling), which requires the presence of chemical bonds and is observable via 1-3 bonds ($\mathcal{H}_J$ in eq. 2.1) [14]. Indirect coupling is a weak magnetic interaction and is usually observed as chemical shift coupling patterns in high-resolution NMR spectra. In solution state, fast molecular motion averages the anisotropic part of the *J*-coupling and only the isotropic part of the *J*-coupling (also termed scalar coupling) is usually observed. Both I-I (homonuclear) and I-S (heteronuclear) *J*-couplings exist and serve as an important route for magnetization transfer in many multidimensional NMR experiments such as in the HSQC experiment [47].

Sometimes, the 1D NMR spectrum is too crowded for signal assignment due to signal overlap. In order to separate overlapping signals, especially for ^{1}H (chemical shift range ~10 ppm), a second dimension is introduced to create a 2D NMR spectrum, which provides improved resolution. With 2D NMR it is also easier to assign and, possibly also, integrate signals. This is especially the case for lignin and related compounds where there is a large distribution of molecular structures that leads to ^{1}H NMR spectra that provide very little information concerning the molecular structures. To overcome this, 2D [^{1}H-^{13}C]-NMR experiments for lignins are widely used as the introduction of the carbon dimension provides sufficient resolution and dispersion to detect lignin structural features [48]. One of the widely used multinuclear NMR experiments is the heteronuclear single-quantum coherence (HSQC) experiment [47] where the polarization is transferred from ^{1}H to X nucleus (e.g. ^{13}C) using an insensitive nuclei enhanced by polarization transfer (INEPT) block [49]. As in the CP experiment, the sensitivity is enhanced by a factor of γ_H/γ_C and the repetition rate is dictated by ^{1}H, but in INEPT the magnetization is transferred from the protons to carbons via *J*-couplings and the effectiveness of this magnetization is more dependent on the *J*-coupling value than direct dipolar couplings. The natural range of $^1J_{CH}$ couplings for organic compounds are in a range of 115-220 Hz [50] and usually a compromise value of around 140-150 Hz is chosen for the [^{1}H, ^{13}C]-HSQC experiment for lignin related materials. The basic HSQC experiment is depicted in Figure 8. Similar to the

CP pulse scheme, an HSQC experiment typically results in non-quantitative data mainly due to variations in *J*-couplings, off-resonance effects, and different relaxation processes. Different HSQC pulse schemes are available for more quantitative data via *J*-coupling compensation [50] [51] [52].

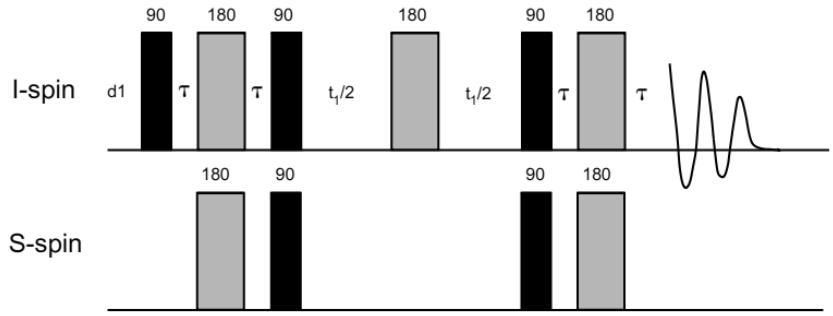

Figure 8 An HSQC NMR experiment without S spin decoupling. The τ values are adjusted according to match the $^1J_{IS}$ couplings ($1/4J_{IS}$), d1 is the repetition time between the pulse trains and t_1 is the evolution period for the S spin. Black and grey rectangles indicate hard rectangular 90º (π/2) and 180º (π) pulses, respectively.

3.4 Quadrupolar coupling

Quadrupolar coupling (C_Q) ($\mathcal{H}_Q$ in eq. 2.1) exists for nuclei with spin I >½ and is caused by the quadrupole moment (eQ) and electric field gradient (EFG) [14]. The quadrupole moment (eQ) is due to asymmetry of the electrical charge in the nucleus and the EFG due to the non-spherical distribution of electrons surrounding the nucleus [32]. When the electron asymmetry is large around the nucleus, the EFG together with quadrupole moment (eQ) results in a very large quadrupolar coupling (C_Q) value [53]. In solid-state NMR, this can result in very broad signal line widths and also affect the nutation frequencies [54]. The degree to which the magnetization is affected by the r. f. pulse is also dependent on this C_Q; for large C_Q the central transition of a quadrupolar nucleus nutates at a higher frequency (Figure 9). In solution state, the quadrupolar interaction is usually averaged to zero in the spectrum but makes a significant contribution to the relaxation of the nucleus [14].

For quadrupolar nuclei in solid-state NMR, the most reliable method for acquiring quantitative data is the direct polarization (DP) technique combined with MAS [55].

Taking into consideration the complete spin-lattice T_1 relaxation of the observed nuclei, the DP technique provides quantitatively reliable signal areas in the NMR spectrum if care is taken when selecting the angle of the excitation pulse. Using direct polarization, an excitation pulse $\pi/2$ (90º) giving maximum signal may be used for spin ½ nuclei, whereas for quadrupolar nuclei ($I > ½$ and large C_Q) short pulses are needed for quantitative results even if a relaxation delay of 5 x T_1 is used. This is due to the faster nutation frequency of the quadrupolar nucleus versus the pulse excitation length (Figure 9).

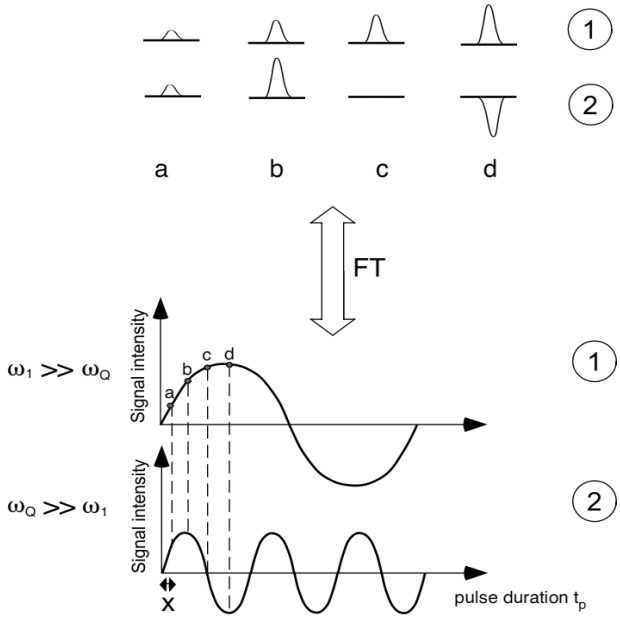

Figure 9 Plot of a signal intensity for the central transition vs. excitation pulse duration (t_p) for spin $I > ½$ in two cases ($\omega_1 >> \omega_Q$(1) and $\omega_Q >> \omega_1$(2)). Only the short pulse (a) duration provides quantitative NMR data in both scenarios. ω_1 is the r. f. nutation frequency and ω_Q is the quadrupolar frequency. Schematic presentation assumes the simple direct polarization technique.

If we have a sample with both small (or zero) and large C_Q, we have nuclei with magnetization nutation profiles 1 and 2 (Figure 9). Only the short excitation pulses provide signal intensities in FT NMR spectra that are quantitatively comparable (marked with x). Therefore, for samples with various quadrupolar interactions only the short direct

excitation pulses should be used to obtain comparable quantitative data [54]. The appropriate maximum pulse length (t_p) may be calculated roughly using the equation:

$$\left(I + \frac{1}{2}\right) \omega_1 t_p \leq \frac{\pi}{6}, \tag{3.4}$$

where ω_1 is the r. f. field strength and t_p excitation pulse duration. For e.g.^{27}Al (I=5/2), this means that the excitation pulse angle should be less than $\pi/18$ ($\leq 10°$) [54].

3.5 Relaxation and nOe

In NMR spectroscopy, there exist mainly two different types of relaxation: longitudinal T_1 (spin-lattice) and transverse T_2 (spin-spin) relaxation. T_1 relaxation is used to define the time of the nuclei to regain the original thermal equilibrium in the z-axis. This z-magnetization recovery is taking place as the nuclei release their energy to the surrounding ''lattice'' (hence the name). Typical T_1 relaxation mechanisms include dipolar interaction ($\mathcal{H}_{DD}$ in eq. 2.1), chemical shift anisotropy ($\mathcal{H}_{CS}$ in eq. 2.1), quadrupolar (for spins I > 1/2) ($\mathcal{H}_{Q}$ in eq. 2.1), spin-rotation ($\mathcal{H}_{SR}$ in eq. 2.1), and also a relaxation mechanism via scalar couplings ($\mathcal{H}_{J}$ in eq. 2.1) exist [14] [32]. In the absence of quadrupolar interactions, usually the dipole-dipole interaction is the dominating mechanisms for the T_1 relaxation. Since the relaxation due to CSA is proportional to $\propto B_0$, its size, in very strong magnetic fields, becomes comparable with direct dipolar couplings [56]. T_1 relaxation is an enthalpic process, whereas the other type of relaxation in NMR spectroscopy, T_2, is merely an entropic process. T_2 relaxation does not involve any energy transfer but defines the process where precessing spins in the xy-plane are losing coherence. Both of these relaxation processes (T_1 and T_2) take place simultaneously and usually follow an exponential process (assuming zero initial magnetization in the z-axis). The T_1 process can be described by:

$$M_z(t) = M_0 \left(1 - e^{-t/T_1}\right) \tag{3.5}$$

And after a 90° ($\pi/2$) pulse, the T_2 process can be described by:

$$M_{x,y}(t) = M_0 e^{-t/T_2} \quad (3.6)$$

where M(0) is the net magnetization at thermal equilibrium, and M (t) magnetization at time position *t*. Relaxation times have an effect on signal intensities in NMR spectra. In order to obtain quantitative NMR data, it is essential to have the correct repetition rate in order to allow enough time for the spins to relax back to equilibrium between the pulses. For instance, if $\pi/2$ (90°) excitation pulses are to be used (e.g. as in cross-polarization), ^{1}H recycle times of 5 X T_1 of spins species with longest T_1 are needed for the recovery of magnetization (>99%) [10]. Too fast, a repetition rate distorts the relative signal intensities in the NMR spectra if different spin species have different relaxation times and one or more of these does not relax back to equilibrium before a subsequent acquisition. Consequently the relative integrals will not reflect the true populations of the different spin species.
The nuclear Overhauser effect (nOe) originates from certain spin transitions (known as cross-relaxation) between different energy levels of a dipolar-coupled pair during T_1 relaxation and may lead to increased or decreased signal intensities in NMR spectra [57] [14]. Since nOe is generated via dipolar modulation (through space) it has a distance dependency of $1/r^6$ and its sign and size depends upon the nuclei and on the molecule rotational correlation time (τ_c) [14] [10] [58]. It is important to consider the effect of the nOe when trying to obtain reliable signal intensities for quantitation. This is especially the case in solution state NMR, where fast molecular tumbling provides the environment for this cross-relaxation to take place, and care must be taken to minimize the effect of nOe when quantitative spectra are required. Typically, this means that in order to obtain quantitative high resolution ^{13}C or ^{31}P NMR spectra, proton decoupling is turned on only for the shortest period of time, i.e. during acquisition to prevent the build-up of the heteronuclear nOe during the recycle time.

In the solid-state, the rigidity of the molecules does not usually provide an environment for dipolar modulation, and consequently heteronuclear nOe is typically not observed. There are exceptions such as some borane adducts [59] and lithium (^{6}Li and ^{7}Li) containing systems [60] [61], where the heteronuclear nOe has been observed as these materials possess fast moving dipolar coupled spins.

4 Applications

4.1 Lignin structure elucidation using *J*-coupling compensated 2D [^{1}H-^{13}C]-HSQC and 1D ^{31}P NMR experiments (PUBLICATION I)

4.1.1. Introduction

The total mass of lignin in softwoods and hardwoods is typically around 25-30 % and 20-25 % [106] whereas in e.g. wheat straw, lignin accounts for 5-15 % [62]. Lignin is a complex heterogeneous biopolymer composed of three main aromatic units linked together by various inter-unit linkages (Figure 10).

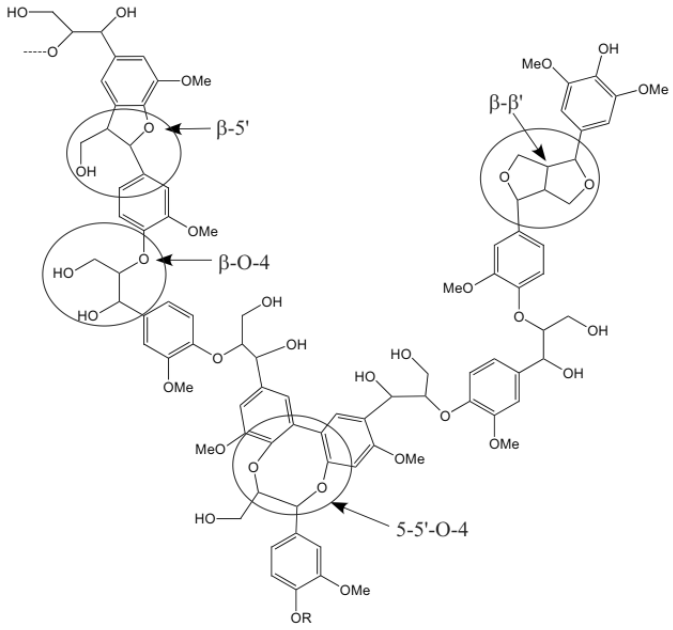

Figure 10 Lignin structure is typically very complex. Example of a part of gross lignin structure, where the aromatic units are linked together via inter-unit linkages; *β'*-O-4 (aryl ether), *β'*-5 (phenylcoumaran), *β-β'* (pinoresinol), and 5-5'-O-4 (dibenzodioxin).

The main aromatic units are *p*-hydroxyphenyl (H), guaiacyl (G), and syringyl (S) units

originating from *p*-coumaryl alcohol, coniferyl alcohol and sinapyl alcohol, respectively (Figure 11).

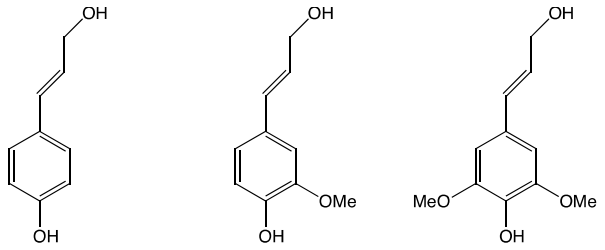

Figure 11 The lignin precursors: *p*-coumaryl alcohol, coniferyl alcohol, and sinapyl alcohol forming lignin aromatic units: *p*-hydroxyphenyl (H), guaiacyl (G), and syringyl (S), respectively.

Aromatic unit composition varies depending upon the plant origin, with softwood (e.g. pine, spruce) lignin mainly composed of G units, together with a small amount of H units, whereas in hardwood (e.g. birch) both G and S units are abundant. The most abundant inter-unit linkages connecting the aromatic units are *β*-O-4 (aryl ether), *β*-5' (phenylcoumaran), *β*-*β′* (pinoresinol), *β*-1'(spirodienone), 5-5'-O-4 (dibenzodioxocin), and 4-O-5' of which *β*-O-4 accounts for 30-40% and 40-50% of the total number of linkages in softwood and hardwood, respectively [63]. Also, *α,β*-diarylether structures have been found in wheat straw lignin [64]. Covalently bound heteropolysaccharides are also usually present in the isolated lignins forming so-called lignin-carbohydrate complexes (LCC) [65] [66]. These carbohydrates may be bound to lignin through phenyl glycoside, ether, or ester linkages [67]. In the literature, the chemical structure of lignin is depicted in different ways [68].

As the NMR spectroscopy is a non-invasive method, it is well suited for providing detailed molecular level information of lignin materials. Especially the 2D [^{1}H, ^{13}C]-HSQC and 1D ^{31}P NMR experiments have widely been used to determine the amounts of inter-unit linkages and other structural features of lignin [50] [69] [70] [71] [72] [73]. This detailed information is needed in the development of a conversion technology exploiting the lignocellulosic materials as a feedstock for producing biofuels and other chemicals.

4.1.2. Materials and methods

For this work lignin samples were isolated from raw wheat straw (MTT Agrifood Research, Jokioinen, Finland) employing the enzymatic mild acidolysis lignin (EMAL) method. The same isolation method was employed before and after steam explosion (SE) treatment [74]. Isolation of EMAL lignin from non-treated and SE treated wheat straw involved the following four main steps: extraction of acetone-soluble material, ball milling, enzymatic hydrolysis of cell wall carbohydrates, and lignin extraction with a mildly acidic dioxane/water mixture. The lignin isolation protocol is explained in more detail in the literature. The model compound tricin (4',5,7-trihydroxy-3',5'-dimethoxyflavone, SelectLab Chemicals GmbH, Bönen, Germany) was used as received.

For the 2D [^{1}H, ^{13}C]-HSQC and HMBC experiments 50 mg of the lignin sample was dissolved in 1 mL DMSO-d_6. NMR experiments were carried out at 303 K on a 600 MHz (^{1}H) Bruker Avance III spectrometer equipped with a cryogenically cooled CPQCI probe head. [^{1}H, ^{13}C]-HSQC experiment was measured using echo/anti-echo time proportional phase incrementation (TPPI) selection, and matched sweep adiabatic pulses, optimized for a ^{13}C sweep width of 200-50 ppm, were used for all 180° ^{13}C pulses [52].

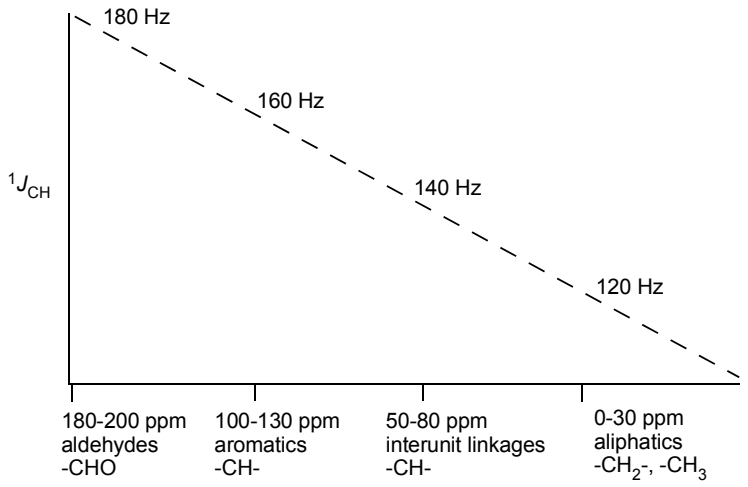

Figure 12 A schematic presentation of $^{1}J_{CH}$ coupling values (dashed line) with respect to chemical shifts and corresponding structural units of lignin. Matched adiabatic sweep compensates for the differences in the transfer delays due to $^{1}J_{CH}$ coupling constants. In this study, the sweep width of 50-200 ppm was optimized neglecting the aliphatic region.

This method should, in principle, compensate for the differences in the $^{1}J_{CH}$ coupling constant (Figure 12), which is one of the main reasons why the [^{1}H, ^{13}C]-HSQC experiment is not considered to provide directly quantitative information [50]. The [^{1}H, ^{13}C]-HMBC experiment was optimized for the long-range couplings (8 Hz) to reveal the connectivity over glycoside bonds. The quantitation was based on the integral areas of G_2 + $S_{2,6}/2$, assuming neither of those carbons would be substituted [69]. This method was chosen as the signals of G and S units are usually well identified in the [^{1}H, ^{13}C]-HSQC spectrum and they all have one attached proton. Similar T_1 relaxation and off-set characteristics are also assumed, as they are part of the globular gross lignin structure. [^{1}H, ^{13}C]-HSQC experiment was also chosen over the more exploited 1D ^{13}C NMR for quantitation in lignins as the inter-unit linkages are not well resolved from the 1D ^{13}C NMR spectrum.

1D ^{31}P{^{1}H} NMR spectra were measured at 293 K using a 500 MHz (^{1}H) Bruker Avance III NMR spectrometer equipped with a 5 mm broadband observe (BBO) probe head. For the quantitative ^{31}P NMR analyses, the studied samples were phosphorylated using the experimental procedure described elsewhere [75]. ^{31}P NMR spectra were measured from freshly prepared samples. The method assumes all free hydroxyl groups in lignin to be phosphorylated and therefore give quantitative information about the distinct lignin structures and functionalities from the ^{31}P NMR spectra. The presence of water in the lignin sample severely downgrades the usability of this method as the phosphorylation reagent vigorously reacts with water. Although not used in this study, Fourier Transformed Infrared Spectroscopy (FTIR) method could be used to follow the content of the free –OH groups in lignin prior to the ^{31}P NMR measurements, similarly as in lignin acetylation in order to dissolve lignin in highly volatile organic solvents [76] [77].

4.1.3. Results and discussion

The inter-unit linkages were determined from the 2D [^{1}H, ^{13}C]-HSQC NMR spectra using H_α-C_α correlation signals (with the exception of H_β-C_β in the α-oxidized β-O-4'structure) and compared to the total C_9 ($0.5S_{2,6}$ + G_2) unit integral (Figure 14). The lignin subunits detected are presented in Figure 13. Based on the integrals, steam explosion alters the wheat straw lignin structure in several ways. The amount of inter-unit linkages and structural characteristics detected in wheat straw lignin before (EMAL) and after the SE

treatment are shown in Table 1.

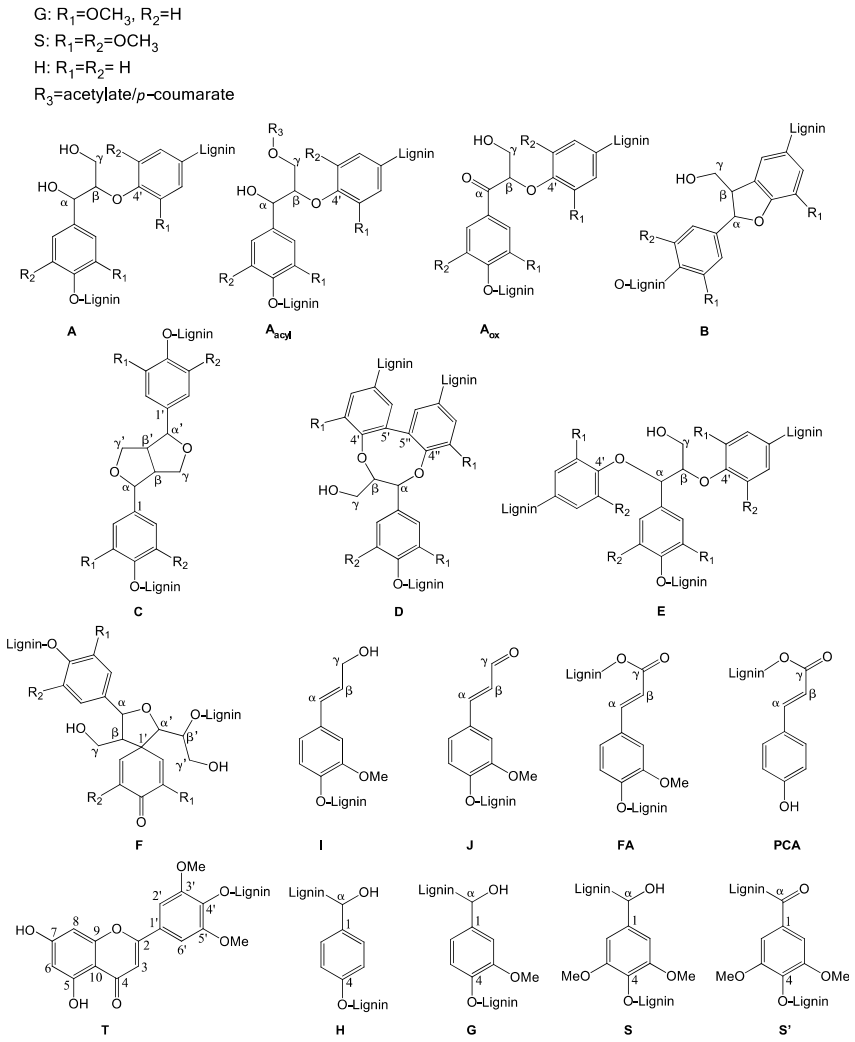

Figure 13 Main lignin structures detected in 2D [^{1}H, ^{13}C]-HSQC NMR. (A) *β*-O-4', (A_{acyl}) *β*-O-4'alkyl-aryl ethers with acylated *γ*-OH, (A_{ox}) Cα-oxidized β-O-4' structure, (B) phenylcoumaran (*β*-5'), (C) resinol (*β*-*β*'), (D) dibenzodioxocin (5-5' –O-4'), (E) *α*,*β*-diarylether, (F) spirodienone (*β*-1), (I) cinnamyl alcohol, (J) cinnamyl aldehyde, (PCA) p-coumarate, (FA) ferulate, (H) p-hydroxyphenyl unit, (G) guaiacyl unit, (S) syringly unit, and (S') Cα-oxidized unit. Reprinted with permission from Heikkinen et al., *Journal of Agricultural and Food Chemistry 43(62).* Copyright (2014) American Chemical Society.

Table 1. Amount of main inter-unit linkages and structural components detected in wheat straw lignin before and after steam explosion treatment from the signals observed in [^{1}H, ^{13}C]-HSQC NMR spectra.

	Wheat straw	
Interunit linkage[a]	**EMAL**	**SE**
β-O-4' (G + S)	66	51
β-O-4' (S)	41	26
β-O-4' (G)	25	25
β-5'	10	16
β-β	5	3
5-5' -O-4'	8	2
β-1 (including SD)	trace	trace
α-oxidized β-O-4' [b]	6	2
α,β-diaryl ethers	3	1
Cinnamyl alcohol	0.7	0.6
Cinnamyl aldehyde	1.4	1.5
Aromatic units [a]		
S/G ratio	0.6	0.4
PCA	11	5
FA	2.7	1.9
PCA/FA ratio	4.0	2.6
Tricin	13	2

[a] Expressed as the number per 100 C_9 units ($0.5S_{2,6} + G_2$).

[b] H_β-C_β correlation signal integral.

Reprinted with permission from Heikkinen et al., *Journal of Agricultural and Food Chemistry 43(62).* Copyright (2014) American Chemical Society.

It was observed that S-type β-O-4' inter-unit linkages were substantially cleaved (36% decrease). This dominating lignin depolymerization reaction is well known in the literature [78] [79]. Another, and perhaps more interesting, reaction was observed in the increase in the amount of phenylcoumaran (β-5') inter-unit linkages after the SE treatment. This reaction, in acidic conditions, has been previously observed in the literature and was attributed to competing repolymerization/depolymerization reactions [80] [81]. Also, a substantial decrease for the cinnamic acids was observed, particularly *p*-coumaric acid, which is known to acylate a portion of *γ*-OH of the lignin side chain in grass.

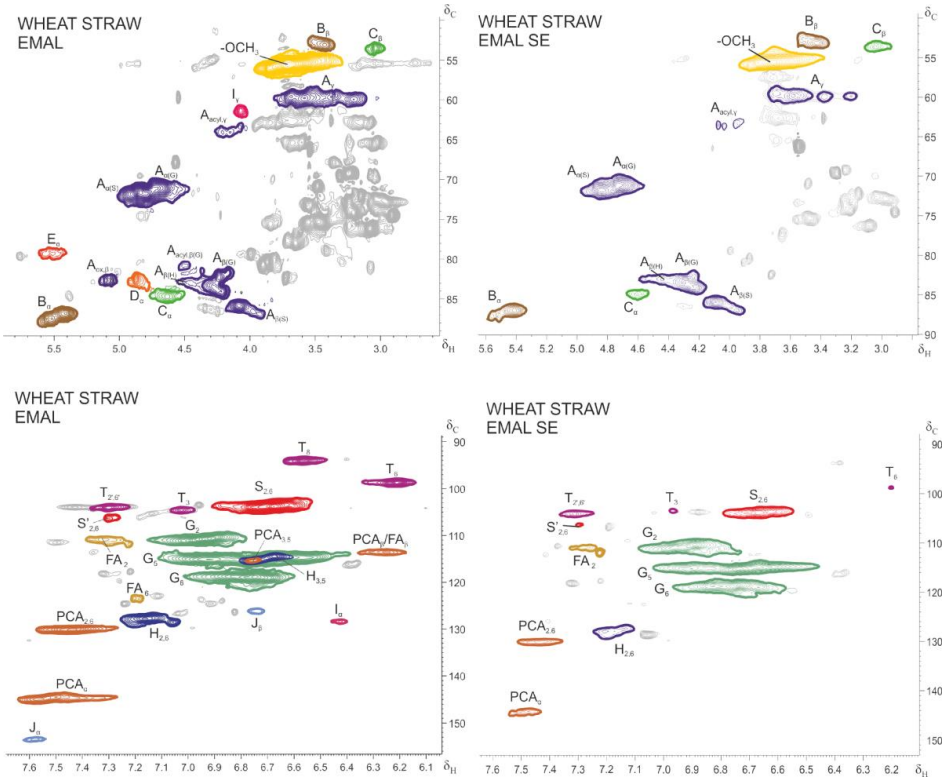

Figure 14 2D [^{1}H, ^{13}C]-HSQC NMR spectra of wheat straw lignin before and after SE treatment. Side-chain and aromatic/unsaturated regions are shown together with inter-unit linkages and main lignin structures assignment. Carbohydrates are colored grey. Signal identification was based on literature and [^{1}H, ^{13}C]-HMBC NMR spectra. [64] [82] Reprinted with permission from Heikkinen et al., *Journal of Agricultural and Food Chemistry 43(62).* Copyright (2014) American Chemical Society.

A significant loss of tricin was observed (85 %). Tricin incorporation in lignin via β-O-4'inter-unit linkages has been demonstrated in the literature. [64] To further elucidate the lignin structure, quantitative 1D ^{31}P{^{1}H} NMR was measured. The ^{31}P{^{1}H} NMR spectra of phosphitylated lignins before and after the SE treatment together with tricin model compound are shown in Figure 15. To verify signals originating from the tricin molecule in the ^{31}P NMR spectra, a model compound was used. As seen from the ^{31}P NMR spectrum, three distinct chemical shifts at 136.40 ppm, 137.67 ppm, and 141.96 ppm are tentatively assigned to 7-OH, 5-OH, and 4'-OH hydroxyl groups, respectively (Figure 15). ^{31}P NMR spectra also confirm the presence of tricin in wheat straw lignin and its partial cleavage in

the SE treatment. Significantly less intense signal of C4'-OH indicates its role in linking to lignin. The quantitative results of the amounts of the tricin molecule before and after the SE treatment were calculated as 0.15 and 0.02 mmol/g of lignin, respectively, based on the C_7-OH signal integral with the assumption that all –OH groups are phosphitylated.

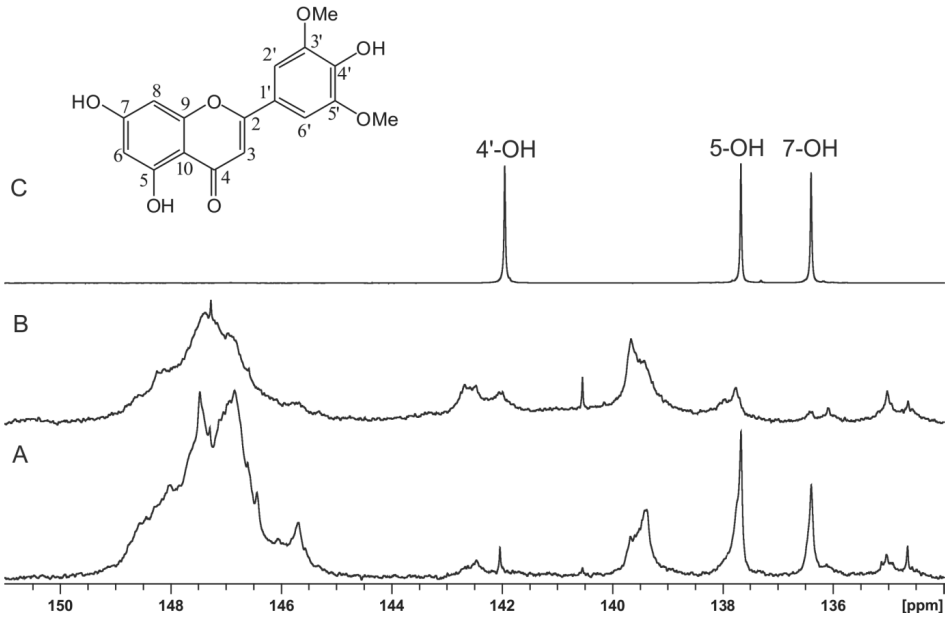

Figure 15 1D $^{31}P\{^1H\}$ NMR spectra of wheat straw lignin before (A) and after SE treatment (B) and tricin model compound (C). The inset shows the molecular structure of tricin with three different OH-groups in the molecule. Reprinted with permission from Heikkinen et al., *Journal of Agricultural and Food Chemistry 43(62).* Copyright (2014) American Chemical Society.

4.2 Zeolite structure elucidation and quantitative Brönsted acid site determination using ^{1}H, ^{27}Al and ^{29}Si MAS NMR experiments (PUBLICATION II)

4.2.1. Introduction

Zeolites are open-framework aluminosilicates, formed from open arrangements of AlO_4^{5-} and SiO_4^{4-} tetrahedra linked by shared oxygen atoms and described by the general oxide formula [83]:

$$M^{x+}_{y/x}[(AlO_2)_y(SiO_2)_{1-y}] \bullet nH_2O, \quad (4.1)$$

where the part within the brackets represents the lattice. Extra-lattice cations (M^{x+}) must be present to preserve electrical neutrality. Additionally, water of hydration is also usually present but is not part of the lattice structure. Catalytic activity of zeolites is generated by changing the extra-lattice cations to H^+ ("acid form") [83]. The process is sketched out in Eq. (4.2)

$$\text{zeolite-}M^{x+} \xrightarrow[\text{"exchange"}]{NH_4^+} \underset{\textbf{ammonium form}}{\text{zeolite-}NH_4} \xrightarrow[\text{"calcine"}]{723\ K} \underset{\textbf{acid form}}{\text{zeolite-}H^+ + NH_3\uparrow} \quad (4.2)$$

The acid form of a zeolite acts as a strong acid catalyst and is used in reactions such as cracking, isomerizations, alkylations and hydrogen transfers [84] [85] [86]. As the acidity and the pore structure of zeolites are unique, they are chosen depending on the reactant used and the desired products. The size- and shape-selective characteristics of the zeolites originate from the unique framework structure and the nomenclature is traditionally based on the unit cells and lattice structure formed therein [86]. Examples of widely employed zeolites include faujasite type (e.g zeolite X and Y) [87] [88], mordenite type (e.g. zeolite beta) [89] [90] and pentasil type (e.g. ZSM-5) [91] [92] lattice structures. One of the interesting application areas where zeolites can be used is the production of aromatics from the biobased feedstock. The zeolites offer the acidic platform and provide the shape selectivity for aromatics production. In this work, the potential of using different zeolite

materials for aromatics production using crude sulphate turpentine (CST) was evaluated. CST is a byproduct formed during a Kraft pulping process of pinewood and contains mainly monoterpenes, which can be converted into other monoaromatics [93].

4.2.2. Materials and methods

Multinuclear solid-state NMR techniques were used to characterize zeolite structures in detail; ^{1}H MAS NMR was used to measure quantitatively the Brönsted acid sites, ^{29}Si MAS NMR to measure the framework Si/Al ratio, and ^{27}Al MAS NMR to reveal the amount of framework (Al_{IV}) and non-framework Al (Al_{VI}). Zeolite catalysts (Molecular Sieve 13X (FAU X), Mordenite (MOR) and Faujasite Y (FAU Y)) were obtained from commercial sources; 13X (FAU X) from Union Carbide and Mordenite (MOR) and Faujasite Y (FAU Y) from Zeolyst. The zeolite material characteristics are shown in Table 2.

Table 2. Structural details of the studied zeolite materials.

Catalyst	Zeolite	SiO_2/Al_2O_3 [a]	Na_2O (wt-%) [a]	BET (m^2/g)	Pore size (Å)
CBV600	FAU Y	5.2	0.2	660	7.44 [b]
CBV21A	MOR	20	0.08	500	7.0 × 6.7 [c]
13X	FAU X	2.5±0.5	9.56	412	7.4 [b]

[a] Value obtained from the manufacturer

[b] See ref [94]

[c] See ref [95]

Reprinted with permission from Linnekoski et al., *Organic Process Research & Development 18*. Copyright (2014) American Chemical Society.

All NMR measurements were carried out at 293 K using an Agilent narrow-bore 600 MHz (^{1}H) NMR spectrometer equipped with a 3.2 mm-o.d. HXY MAS probe head. For the ^{1}H MAS NMR experiments, the samples were dehydrated at 673 K for 4 h under dry nitrogen gas flow. After dehydration, the samples were loaded into 3.2 mm-o.d. zirconia rotors under nitrogen atmosphere. For each ^{1}H NMR spectra, 128 transients were accumulated with 2.85 μs (π/2) pulse, 30 s recycle delay, and a MAS rate of 20 kHz [96] [103]. For the quantitative OH group determination, a full rotor of Q8M8 (octakis-(trimethylsiloxy)silesquioxane, Chymos GmbH, CAS No. 51777-38-9) was used as an external standard. The area of the spectrum of a known weight of reference (Q8M8) was

compared with the spectrum area of a known weight of the unknown samples (spin counting) and the amount of OH groups per gram was determined (Table 3) [97].

^{27}Al MAS and ^{29}Si MAS NMR experiments were carried out on samples in the hydrated form. For the ^{29}Si MAS NMR measurements, 20,000 transients were accumulated using 3 μs pulse (π/4), 10 s recycle delay and MAS rate of 10 kHz [98]. The framework Si/Al ratios were determined (Table 4) from the ^{29}Si MAS NMR spectra using the following equation [99]:

$$\frac{Si}{Al} = \sum_{n=0}^{n=4} I\ Si(nAl) \,/\, \sum_{n=0}^{n=4} \frac{n}{4}\ I\ Si(nAl), \tag{4.3}$$

where n in Si(nAl) is determined by the number of Al surrounding Si in the framework and I Si(nAl) is the peak area of each Si(nAl) species in the ^{29}Si MAS NMR spectrum (see Figure 17 as an example) [100]. The equation 4.3 can be used to evaluate the Si/Al ratio when the Loewenstein's rule is fulfilled, i.e. no Al-O-Al bond is allowed [101]. ^{27}Al MAS NMR spectra were measured to observe ratios of different Al species. In the ^{27}Al MAS NMR experiments, 4000 transients were accumulated using a short 1 μs pulse, 2 s recycle delay, and MAS rate of 20 kHz [102]. In all cases, a background signal, run under identical conditions with an empty rotor, was subtracted from the spectra. NMR spectra were processed using the GSim software. The chemical shift assignment was carried out according to the literature [103] [104].

4.2.3. Results and discussion

All the studied zeolites are large pore zeolites (>7 Å) and possess several types of acid sites, which participate in the reactions and affect the reactivity. In this study, ^{1}H MAS NMR was used to measure quantitatively the Brönsted acid sites (i.e. bridging SiOHAl groups) from these zeolites. The ^{1}H MAS NMR spectrum of faujasite Y (Si/Al 8.4) is shown in Figure 16.

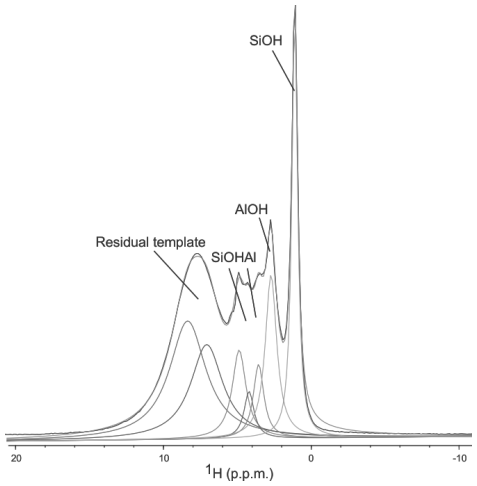

Figure 16 ^{1}H MAS (20 kHz) NMR spectrum of zeolite FAU Y (Si/Al 8.4) with signal assignments. Peak deconvolution was carried out using GSim [128]. Reprinted with permission from Linnekoski et al., *Organic Process Research & Development 18.* Copyright (2014) American Chemical Society.

Based on the results, FAU Y shows the highest number of Brönsted acid sites (450 µmol/g) whereas FAU X (70 µmol/g) has the lowest which is tentatively assumed to originate due to the higher Na_2O amount in FAU X. This is not removed during the dehydration process. Also, a broad signal at 7-8 ppm was observed in ^{1}H NMR spectrum and assigned to residual template (i.e. hydrocarbons within the zeolite structure) as the samples were not calcined in air to drive this off prior to ^{1}H NMR measurements. Whereas FAU Y and FAU X showed moderate amounts of residual template, the ^{1}H MAS NMR spectrum of MOR was dominated by it, and an accurate acid site determination was not possible. Since the OH group determination is based on the use of an external standard (Q8M8) and the signal deconvolution was needed in order to separate different hydroxyl groups, an error marginal of 5 % was estimated for the OH and H amounts.

Table 3. Quantitative OH amounts and the total number of H in each sample based on ^{1}H MAS NMR spectra.

	Amount (μmol/g)± 5%				
Zeolite	**Acid OH**	**AlOH**	**SiOH**	**Residual template**	**Total amount of H**
FAU Y	450	262	489	1388	2589
MOR	n.m.	n.m.	n.m.	n.m.	11580
FAU X	68	73	46	1785	1972

Reprinted with permission from Linnekoski et al., *Organic Process Research & Development 18*. Copyright (2014) American Chemical Society.

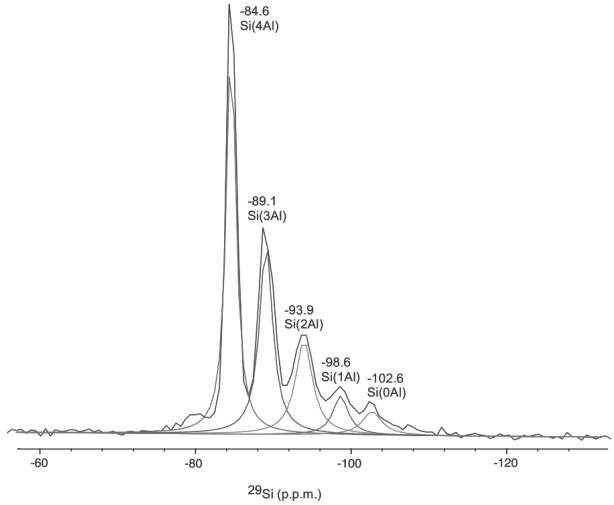

Figure 17 ^{29}Si MAS (10 kHz) NMR spectrum of FAU X (Si/Al 1.4) with chemical shifts and signal assignations. Peak deconvolution was carried out using GSim [128]. Reprinted with permission from Linnekoski et al., *Organic Process Research & Development 18*. Copyright (2014) American Chemical Society.

^{27}Al MAS NMR spectra were measured to observe the ratios of different Al species (Table 4). Three main different types of Al species were observed and assigned according to their isotropic chemical shift range: four-coordinated framework aluminum ($Al(IV)_{FR}$) around 75-50 ppm, five-coordinated non-framework aluminum ($Al(V)_{NFR}$) around 40-30 ppm and six-coordinated non-framework aluminum ($Al(VI)_{NFR}$) around 20-0 ppm (Figure 18)

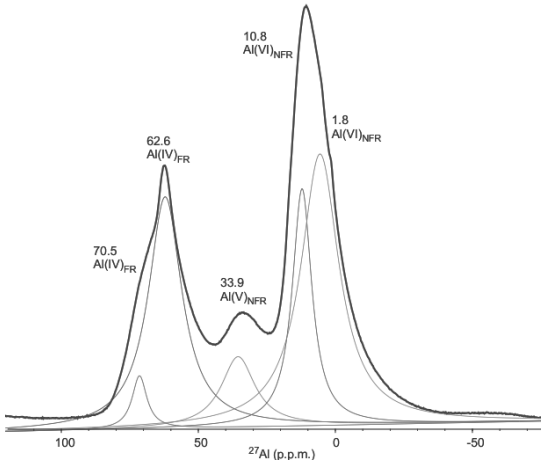

Figure 18 ^{27}Al MAS (20 kHz) NMR spectrum of FAU Y (Si/Al 8.4) with chemical shifts and signal assignations. The central transition signal of ^{27}Al (I=5/2) is shown. Peak deconvolution was carried out using GSim [128]. Reprinted with permission from Linnekoski et al., *Organic Process Research & Development 18.* Copyright (2014) American Chemical Society.

[105]. The results show that in FAU Y 38% of the total amount of Al is located in the framework whereas the framework Al in FAU X is 97% (Table 4). The framework Al is directly proportional to the amount of Brönsted acid sites (bridging SiOHAl). Although FAU X shows the highest $Al(IV)_{FR}$ but lowest acid amounts, is due to fact that this sample had so much Na present which take the place of the H^+ acid sites. In dealumination/realumination processes, for example in dehydration pretreatment, ^{27}Al NMR can be used to follow how the acid sites change. In this work, ^{27}Al NMR data was only used qualitatively and to support the conclusions.

Table 4. Si/Al ratios and the percentages of different Al species of the studied zeolite catalysts.

Zeolite	**SiO_2/Al_2O_3**[a]	**SiO_2/Al_2O_3** [b]	**$Al(IV)_{FR}$**[c]	**$Al(V)_{NFR}$**[c]	**$Al(VI)_{NFR}$**[c]
FAU Y	8.4	5.2	37.9	8.4	53.7
MOR	15.7	20	34.6	38.6	26.8
FAU X	1.4	2.5	96.9	0.1	3.0

[a] Calculated based on ^{29}Si MAS NMR spectra using eq. 4.3

[b] Value obtained from the manufacturer

[c] Evaluated based on ^{27}Al MAS NMR spectra

Reprinted with permission from Linnekoski et al., *Organic Process Research & Development 18*. Copyright (2014) American Chemical Society.

Based on the results, the FAU Y gave the best selectivity for the wanted *p*-cymenes. FAU Y shows the highest Brönsted acidity from the three tested zeolites and in this case, seemed to be best suited for the conversion. Zeolites possess different types of acid sites and with different strengths, which affect the reactivity and participate in the reactions. The presence of template molecules may harm the catalyst operation by interfering with the acid sites. Also, the amount of Brönsted acid sites in these catalysts is probably higher than the measured value as the template severely affects the ^{1}H MAS NMR spectrum and complicates the peak deconvolution. However, the zeolite materials seem to be suitable for the aromatics production using CST as a starting material.

4.3 Determining the degree of substitution of modified cellulose materials with ^{13}C CP/MAS NMR (PUBLICATION III and IV)

4.3.1. Introduction

Cellulose comprises around 40-45% of the dry weight of wood. [106] Cellulose is a linear polysaccharide consisting of glucose units linked by (1→4)-β-glycosidic linkages (Figure 19). The (anhydro)glucose units (AGU) are rotated 180° with respect to each other, so that (anhydro)cellobiose is the smallest structural element of cellulose. As the glucose units contain hydroxyl groups (six per (anhydro)cellobiose), the cellulose chains form both intra- and intermolecular hydrogen bonds. This strong hydrogen-bonding network affects the chemical and physical properties of cellulose; celluloses are usually water insoluble with increasing degree of polymerization (DP), and favor crystallization and formation of fibrillar structures [107] [108]. The number of polymerized glucose units (DP) varies according to the origin of the cellulose and for some bacterial celluloses can be as high as 10,000 [109].

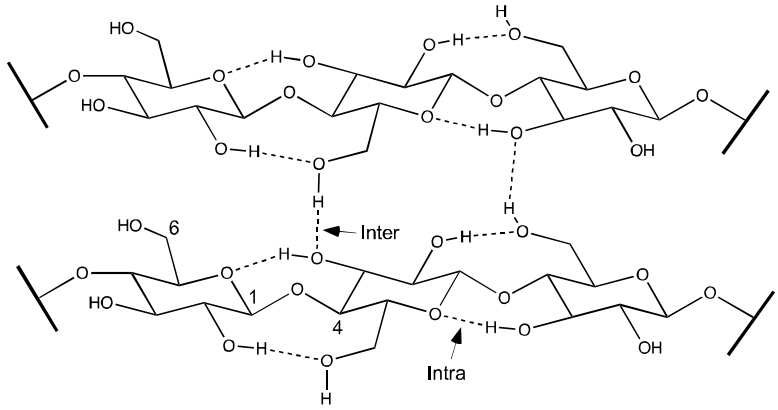

Figure 19 A schematic view of cellulose polymer, where the intra- and intermolecular hydrogen bonds are shown. The hydrogen-bonding network is different between cellulose polymorphs.

Cellulose has at least six polymorphs, designated as I, II, III_I, III_{II}, IV_I and IV_{II} [110]. The crystalline form I is the native form of cellulose (produced by biosynthesis in higher plants) and is found as a mixture of two different polymorphs, I_α and I_β [111]. Other crystalline

forms may be obtained from the native form of cellulose I but cellulose II has been found forming natively in some mutant bacterial strains [112] [113]. The arrangement of cellulose chains in crystalline form I have a parallel chain direction (I_α and I_β have different hydrogen bonding patterns due to different unit cells), whereas in cellulose II, thermodynamically the most stable form of cellulose, the arrangement is antiparallel. Upon heating, the native crystalline form I of cellulose also tends to form the more stable I_β form [114]. The non-crystalline part of cellulose is usually named amorphous cellulose.

Cellulose fibrils, with varying diameters, are potential molecules for composite materials ranging from packaging applications to building materials [115] [116]. For the composite applications, hydrophobicity is introduced into the fibrillar structure. This is usually done via esterifications and etherifications of the hydroxyl groups within the cellulose and to produce the corresponding derivatives of cellulose [117] [118]. Solid-state ^{13}C NMR spectroscopy is widely used to observe and measure the modification degree, i.e. the degree of substitution (DS) of these cellulose derivatives [119] [120] [121] [122]. ^{13}C NMR can also directly identify the changes in cellulose fibril crystallinity upon chemical modifications, making it an invaluable technique especially for studying microfibrillar cellulose (MFC) and nanofibrillar cellulose (NFC) modified materials [123] [124].

4.3.2. Materials and methods

^{13}C CP/MAS NMR was used to determine the DS from various types of cellulosic materials. All cellulose was obtained from UPM-Kymmene Oy. Hydroxypropyl cellulose (HPC) and the cellulose esters were prepared according to procedures described in the literature [125] [126].

All samples were dried under vacuum overnight before the NMR analysis. The prepared modified cellulose samples were analyzed using ^{13}C NMR. The ^{13}C CP/MAS NMR spectra were measured using a Chemagnetics 270 MHz (^1H) NMR instrument equipped with a 6 mm MAS NMR probe head. For all the samples, 20,000 transients were accumulated using a 2 or 3 ms contact time, a 3 s recycle delay and a MAS rate of 5 kHz.

4.3.3. Results and discussion

^{13}C CP/MAS NMR was used to determine the degree of substitution (DS) and to observe

changes in fibrillar structure. In theory, the maximum DS value can be 3 as there are three –OH functionalities in each glucose unit. The characteristic cellulose signals, and carbon moieties from the modified cellulose fibrils could be identified from the ^{13}C NMR spectra. As an example, ^{13}C CP/MAS NMR spectrum of NFC butyrate (DS_{NMR} = 0.2) is shown in Figure 20. For the HPC, the DS was determined by comparing signal area of the methyl and the C1 signal of cellulose with the aid of peak deconvolution using Gaussian line shapes [127]. For the NFC esters, the DS was determined by comparing the signal area of the acyl carbons with the areas of the cellulose carbons. For the MFC hexanoate esters, the DS was determined comparing the signal area of the carbonyl and the α-methylene signals and the C1 signal of cellulose with the aid of peak deconvolution using Gaussian line shapes. The obtained DS values were compared with the XPS data (Table 5 and Table 6). Although the data from NMR is not strictly quantitative, due to the CP dynamics, they can be compared relatively when comparing the same type of groups in the NMR spectra. In this study the obtained DS values are compared in relation to other samples in the same series. For the NFC esters (Table 5), the DS values are basically the same, with the exceptions of palmitate and butyrate, within the error marginal.

Table 5. Obtained degrees of substitution (DS) of NFC esters determined with XPS and NMR methods.

Sample	DS ± 0.05 (XPS)	DS ± 0.05 (NMR)
NFC butyrate	0.4	0.2
NFC butyrate[a]	0.1	0.1
NFC palmitate	0.3	0.1
NFC palmitate[a]	0.2	0.1
NFC hexanoate[b]	0.8	0.7
NFC benzoate	0.3	0.2
NFC naphtoate	0.4	0.3
NFC diphenyl acetate	0.8	0.7
NFC stearate[b]	0.7	0.6

[a] Reaction conducted in acetone

[b] 375 mmol of the corresponding acid chloride was used in the preparation

XPS detects mainly the surface of the cellulose and assumes the structure to be uniform throughout the fiber. However, NMR is a bulk method and measures the bulk of the structure. The results imply that there is a uniform distribution of modified species within the molecular structure, and that palmitate and butyrate esters also show small amounts of non-uniform distributions. On the other hand, DS values obtained for HPC and MFC hexanoate esters (Table 6) are different.

Table 6. Degrees of substitution (DS) of HPC and MFC hexanoate esters determined with XPS and NMR methods.

Sample	**DS ± 0.05 (XPS)**	**DS ± 0.05 (NMR)**
HPC1	0.5	0.5
HPC2	0.1	0.1
MFC hexanoate 1	1.4	0.6
MFC hexanoate 2	1.3	0.6
MFC hexanoate 3	1.3	0.6
MFC hexanoate 4	1.8	0.7
MFC hexanoate 5	1.5	0.7
MFC hexanoate 6	1.9	0.7
MFC hexanoate 7	1.6	0.7

The HPC samples imply a uniform distribution of modified species within the molecular structure, whereas the MFC hexanoate esters are mainly modified on the surface of the fibrillar structure.

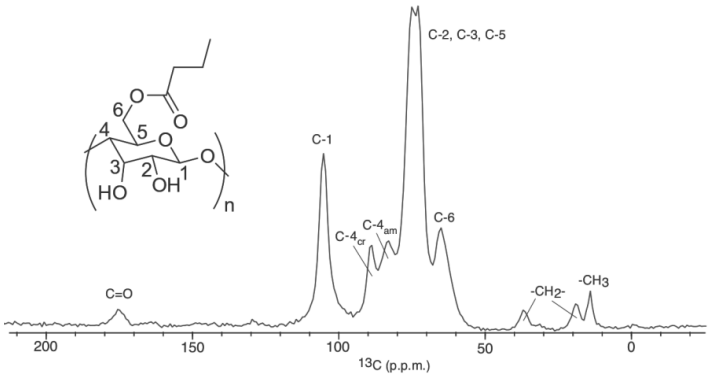

Figure 20 ^{13}C CP/MAS NMR spectrum of NFC butyrate (DS = 0.2) with signal assignments. Cellulose assignments are marked with C-1 to C-6 (Cr indicate crystalline and am amorphous). Butyrate assignments are marked with C=O, -CH_2-, and -CH_3. Chemical structure illustration shows an example where the cellulose polymer (n = number of glucose units) is modified to C-6 position. NMR spectrum was processed using GSim software. [128] Adapted with permission from Vuoti et al., *Cellulose 20.* Copyright (2013). Springer Science Business Media Dordrecht.

4.4 Metal-donor interaction elucidation in Ziegler-Natta catalysts using chemical shift anisotropy data from ^{13}C CP/MAS NMR experiments (PUBLICATION V)

4.4.1. Introduction

Ziegler-Natta (ZN) catalysts are advanced catalysts used for polymerization of olefins, especially polypropylene (PP) [129]. The composition of an active ZN is usually based on a $MgCl_2/TiCl_4$/electron donor system (internal/external donors) and a cocatalyst (e.g. $AlEt_3$). The role of the donor(s) is to regulate the stereochemistry and molecular weight distribution (MWD) of the polymerization product. [130] The ZN catalysts are named after the used electron donor compounds: third generation (benzoate), fourth generation (phthalate) and fifth generation (diether) [131]. As the electron donor plays a vital role in catalyst performance structural information regarding its interactions within the catalyst system is needed to develop new catalyst modifications.

4.4.2. Materials and methods

In this study, the spinning sideband (ssb) pattern was utilized for the characterization of metal-donor interaction in active ZN systems via the observation of the carbonyl moiety of the donor in ^{13}C CP/MAS NMR spectra using low MAS rates. At low MAS rates, the spectrum gives spinning sideband patterns formed by incomplete CSA removal. For individual chemical shifts, three principal components (δ_{11}, δ_{22}, δ_{33}) can be derived (Figure 21).

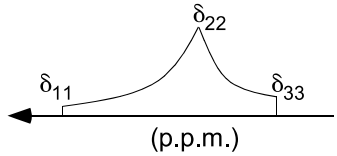

Figure 21 Principal components describing CSA.

The principal components follow the high frequency positive order ($\delta_{11} > \delta_{22} > \delta_{33}$) and the isotropic chemical shift (δ_{iso}) can be simply calculated $\delta_{iso} = 1/3(\delta_{11}+\delta_{22}+\delta_{33})$ [132]. The anisotropy value (δ_{aniso}) describes the largest deviation from the centre of gravity and can be described by $\delta_{aniso} = \delta_{11} - (\delta_{22} + \delta_{33})/2$. The asymmetry parameter (η) describes the shape

of the spinning sideband pattern based on the deviation from axially symmetry. The asymmetry parameter can be calculated as $(\delta_{33}-\delta_{22})/(\delta_{11}-\delta_{iso})$ and hence $0 \leq \eta \geq 1$ [11] [133] [134] [135] [136]. The CSA parameters (δ_{aniso} and η) were obtained from the (δ_{11}, δ_{22}, δ_{33}) values according to the Haeberlen convention using an online converter [137]. Composition of the studied Ziegler-Natta catalysts and model compounds are shown in Table 7. Model compounds (a-e) are based on two-component systems (donor and $TiCl_4/MgCl_2$) whereas active ZN catalysts (a-d) contain both donor(s), $TiCl_4$ and $MgCl_2$ with varying amounts. The chemical structures of the donor compounds used in the studied materials are shown in Figure 22.

Table 7. Composition (donor molar ratio relative to Ti/Mg) of the studied ZN catalysts and model compounds.

ZN catalyst	Donor[a]	Donor	Ti	Mg
Model a	DEP	1	1	-
Model b	EBE	1	1	-
Model c	DEP/DEHP	0.5/0.5	1	-
Model d	DEP	0.075	-	1
Model e	EBE	0.1	-	1
Catalyst a	DEP	0.05	0.05	1
Catalyst b	EHBE	n.m.[b]	n.m.	n.m.
Catalyst c	DEHP	0.09	0.1	1
Catalyst d	DiBP	0.1	0.1	1

[a] DEP = diethyl phthalate, EHBE = 2-ethylhexyl benzoate, DEHP = bis(2-ethylhexyl) phthalate, EBE = ethylbenzoate, DiBP = di-isobutyl phthalate.

[b] n.m. = not measured

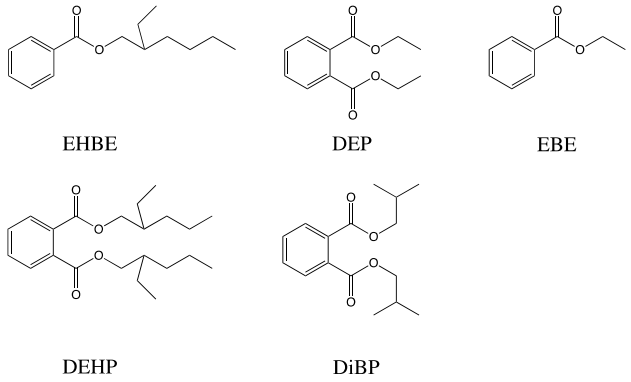

Figure 22 Chemical structures of the donor compounds used in this study.

For the solid-state ^{13}C NMR measurements, samples were dried in vacuo at 60 °C and loaded into 6 mm-o.d. zirconia rotors with a push-on KEL-F cap under nitrogen atmosphere. All ^{13}C NMR measurements were carried out using a Chemagnetics 270 MHz (^{1}H) NMR spectrometer. The ^{13}C NMR spectra were acquired at 298 K with variable-amplitude (VA) cross-polarization (CP) MAS sequence with carbon background suppression [138] [139]. For all the samples, 17,000 transients were accumulated using a 5 ms contact time and a 3 s recycle time. For the CSA studies, low MAS rates between 1.4 and 1.8 kHz were used to reveal the spinning sideband pattern. The ordinary ^{13}C CP/MAS experiments were carried out using MAS rates between 4 and 5 kHz.

4.4.3. Results and discussion

Even though ^{13}C CP/MAS revealed the characteristic signals of the studied samples, the isotropic chemical shifts revealed no information of the donor-metal interaction in this sample series. However, using the principal component data in combination with the CSA calculation it was possible to obtain the anisotropy and asymmetry parameters. ^{13}C CP/MAS NMR spectra of $TiCl_4$/DEP using MAS rate 4.4 kHz (left) and 1.4 kHz (right) are shown in Figure 23.

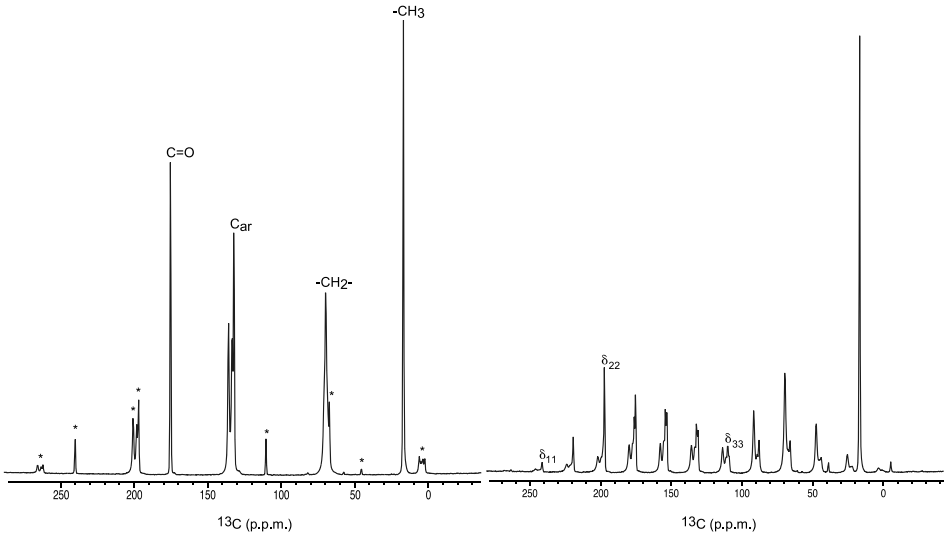

Figure 23 ^{13}C CP/MAS NMR spectra of $TiCl_4$/DEP using MAS rate of 4.4 kHz (left) and 1.4 kHz (right). Characteristic carbon signals (left) and the approximate principal components for the carbonyl moiety (right) are shown. Spinning sidebands are marked with asterisks. Spectrum was processed using GSim software [128]. Reprinted with permission from Heikkinen et al., *Solid State Nuclear Magnetic Resonance 43-44*. Copyright (2012) Elsevier Inc.

Based on the experimental data (Table 8) we postulated that the sign of the anisotropy δ_{aniso} (+/−) indicates to which metal (Mg/Ti) the carbonyl of the donor molecule is coordinating: a negative value indicates coordination to Ti and positive to Mg. We also found out that based on the asymmetry parameter value (η) both model compounds and active ZN catalysts can be divided into two classes: samples with η value near 0.5 and samples with η value near 1. As the η value stems from the symmetry of electrons around the carbonyl moiety, we concluded that higher asymmetry values indicate more complex interactions, i.e. larger variety of interactions whereas asymmetry values close to 0.5 indicate interaction modes taking place in a simple manner.

Table 8. Anisotropy data for the studied model compounds and ZN catalysts derived from low MAS NMR data.

Compound	δ_{11} (ppm ± 0.3)	δ_{22} (ppm ± 0.3)	δ_{33} (ppm ± 0.3)	δ_{iso}(ppm ± 0.3)	δ_{aniso} (ppm ± 0.3)	δ_{iso} experimental (ppm ± 0.2)	η (± 0.01)
Model a	241.1	197.3	109.6	182.7	−109.6	175.3	0.60
Model b	240.9	196.0	106.3	181.1	−112.1	173.6	0.60
Model c	232.1	194.0	117.3	181.1	−95.8	175.2	0.60
Model d	239.5	148.7	103.0	163.7	+113.7	171.6	0.60
	237.5	146.7	101.3	161.9	+113.5	169.6	0.60
Model e	223.4	171.6	120.7	171.9	+77.3	171.5	0.99
Catalyst a	239.4	174.1	110.2	174.6	+97.2	172.8	0.99
Catalyst b	215.0	171.4	128.2	171.5	+65.2	171.4	1.00
Catalyst c	222.5	148.5	124.0	165.0	+86.3	173.6	0.43
Catalyst d	241.8	150.6	106.1	166.1	+113.5	173.4	0.59

It seems that exploitation of the low MAS ^{13}C NMR in combination with CSA calculations can be a promising tool for obtaining detailed information within donor-transition metal interaction in active ZN catalyst materials. Further studies with a more complete catalyst series together with prediction of CSA parameter from density functional theory (DFT) are needed to fully understand the CSA results and to reveal the full potential of CSA in the characterization of ZN catalysts. A methodology used previously only for model compounds [140] could now be applied to more complex catalyst systems used in polypropylene polymerization.

5 Conclusions

NMR spectroscopy provides quantitative information of materials at the atomic level in a manner that cannot be obtained with any other existing analytical tool. The wide applicability of NMR spectroscopy has been demonstrated in this study to be suited for different types of materials covering lignin, cellulose, zeolites and ZN catalysts. Much of the unique information that is provided by NMR is due to the fact that it is a bulk method and is non-destructive. This is especially important factor among lignin research where the isolation process already alters the heterogeneous polymeric structure of lignin and further cleavage is unwanted. The detailed structural information taking place in wheat straw lignin upon steam explosion using 1D and 2D NMR techniques was shown. According to the NMR data, the main reactions of lignin were the cleavage of β-O-4 linkages and the formation of β-5 linkages upon SE. Confirming the presence of tricin and postulating the means to calculate the amount of tricin in the lignin sample using ^{31}P NMR experiment was conducted. The 2D NMR data suggested almost total removal of tricin and significant reduction of G-O-S units.

The fact that NMR is a bulk method means it also provides tools for obtaining key information (degree of substitution, crystalline/amorphous) of modified cellulosic materials in the solid-state without sample degradation. This kind of information is very important in the development of new value-added chemicals and compounds.^{13}C CP/MAS NMR experiments were used to calculate the DS values of several modified NFC samples and comparison of the results with XPS was carried out. The DS values derived from NMR spectra were lower compared to XPS, most likely due to the surface specificity of the XPS technique.

Information throughout the chemical molecular structure is significant also for the three-dimensional structures of alumina silicate materials such as zeolites, where the amount of acid sites and the overall acidity play a big role defining the catalyst properties. The combination of direct polarization ^{1}H, ^{27}Al and ^{29}Si MAS NMR experiments provided useful structural information about the catalyst and quantitative information concerning the Brönsted acid sites. There are other analytical techniques available as well, e.g. the FTIR, which can be used to monitor the acid OH groups directly, but is not usually quantitative, and primarily observes the surface species. FTIR of probe molecules can also be carried

out, but again, quantitation can be problematic, and not all acid sites are necessarily occupied by the probe molecule.

The influence of magnetic interactions in solution and solid-state define the information that is obtainable from the NMR spectrum. The obtainable spectral resolution in solid-state is usually lower than in the liquid state due to the presence of anisotropic interactions, which are not averaged out. Due to this, several methods, such as MAS and high-power decoupling are typically employed in solid-state NMR to ensure higher spectral resolution and to mimic solution state conditions. However, valuable information can sometimes be derived only in the presence of these anisotropic interactions as shown in the study for ZN catalysts. The sign of the chemical shift anisotropy value and the size of the asymmetry values clearly depends on the coordinating metal.

Therefore the choice of NMR experiment is important for realizing the full potential of the quantitative information available for a particular type of material under study.

BIBLIOGRAPHY

[1] Rabi, I. I., Zacharias, J. R., Millman, S., Kusch, P. (**1938**) A new method of measuring Nuclear Magnetic Resonance. *Physical Reviews 53*, 318.

[2] Cooley, J. W., Tukey, J. W. (**1965**) An algorithm for the Machine Calculation of Complex Fourier Series. *Mathematics of Computation 19*, 297-301.

[3] Ernst, R. R., Anderson, W. A. (**1966**) Application of Fourier Transform Spectroscopy to Magnetic Resonance. *Review of Scientific Instruments 37*, 93-102.

[4] Andrew, E. R., Bradbury, A., Eades, R. G. (**1958**) Nuclear magnetic resonance spectra from a crystal rotated at high speed. *Nature 182*, 1659.

[5] Pines, A., Gibby, M. G., Waugh, J. S. (**1972**) Proton-enhanced nuclear induction spectroscopy. A method for high resolution NMR of dilute spins in solids. *Journal of Chemical Physics 56*, 1776-1777.

[6] Hartmann, S. R., Hahn, E. L. (**1962**) Nuclear Double resonance in the rotating frame. *Physical Reviews 128*, 2042.

[7] Mehring, M., Pines, A., Rhim, W. K., Waugh, J. S. (**1971**) Spin-decoupling in resolution of chemical shifts in solids by pulsed nmr. *The Journal of Chemical Physics 54*, 3239-3240.

[8] Stejskal, E. O., Schaefer, J., Waugh, J. S. (**1977**) Magic-angle spinning and polarization transfer in proton-enhanced NMR. *Journal of Magnetic Resonance 28*, 105-112.

[9] Croasmun, W. R., Carlson, R. M. K. (**1994**) Two-dimensional NMR Spectroscopy: Applications for Chemists and Biochemists 2nd ed., John Wiley & Sons, inc.

[10] Claridge, T. D. (**1999**) High-Resolution NMR Techniques in Organic Chemistry 3rd ed., Vol. 19 of Tetrahedron Organic Chemistry Series, Elsevier Ltd.

[11] Mehring, M. (**1983**) Principles of High Resolution NMR in Solids, 2nd edn. Springer, Berlin.

[12] Cavanagh, J., Fairbrother, W. J., Palmer, A. G., Rance, M., Skelton, N. J. (**2007**) Protein NMR Spectroscopy: Principles and Practise, Elsevier Academic Press.

[13] Duer, M. J. (Eds.) (**2001**) Solid State NMR Spectroscopy: Principles and Applications, Wiley-Blackwell.

[14] Levitt, M. H. Spin Dynamics: Basics of Nuclear Magnetic Resonance, John Wiley & Sons, Ltd. **2001**.

[15] Keeler, J. (**2005**) Understanding NMR Spectroscopy, Chichester, England, Hoboken, NJ, Wiley.

[16] Aue, W. P., Bartholdi, E., Ernst, R. R. (**1976**) Two-dimensional spectroscopy. Application to nuclear magnetic resonance. *The Journal of Chemical Physics 64*, 2229-2246.

[17] Wider, G., Dreier, L. (**2006**) Measuring protein concentration by NMR Spectroscopy. *Journal of the American Chemical Society 128*, 2571-2576.

[18] Burton, I. W., Quilliam M. A., Walter, J. A. (**2005**) Quantitative 1H NMR with external standards: Use in preparation of calibration solutions for algal toxins and other natural products. *Analytical Chemistry 77*, 3123-3131.

[19] Tredwell, G. D., Behrends, V., Geier, F. M., Liebeke, M., Bundy, J. G. (**2013**) Between-Person comparison of metabolite fitting for NMR-based quantitative metabolomics. *Analytical Chemistry 83*, 8683-8687.

[20] Koskela, H., Kilpeläinen, I., Heikkinen, S. (**2005**) Some aspects of quantitative 2D NMR. *Journal of Magnetic Resonance 174*, 237-244.

[21] Koskela, H. (**2009**) Quantitative 2D NMR studies. *Annual Reports on NMR Spectroscopy 66*, Webb, G. A. (Ed.) Academic Press, Chapter 1, 1-31.

[22] Axelson, D. E., Mathieu, P. (**1983**) Carbon-13 NMR of Polyethylenes: Correlation of the Crystalline Component T1 with Structure. *Journal of Polymer Science: Polymer Physics Edition 21*: 2319-2335.

[23] Pines, A., Gibby, M. G., Waugh, J. S. (**1973**) Proton-enhanced NMR of dilute spins in solids. *The Journal of Chemical Physics 59*, 569-590.

[24] Atkins, P., de Paula, J. Atkin's Physical Chemistry 7th Ed., Oxford University Press, **2002**.

[25] Abragam, A., Goldman, M. (**1976**) Principles of Dynamic Nuclear Polarization. *Reports on Progress in Physics 41*, 395-467.

[26] Ardenkjaer-Larsen, J., Fridlund, B., Gram, A., Hansson, G., Hansson, L., Lerche, M., Servin, R., Thaning, M., Golman, K., (**2003**) Increase in signal-to-noise ratio of >10,000 times in liquid-state NMR. *Proceedings of the National Academy of Sciences of the United States of America 100*, 10158-10163.

[27] Styles P., Soffe, N. F., Scott, C. A., Crag, D. A., Row, F., White, D. J., White, P. C. J. (**1984**) A high-resolution NMR probe in which the coil and preamplifier are cooled with liquid helium. *Journal of Magnetic Resonance 60*, 397–404.

[28] Kovacs, H., Moskau, D., Spraul, M. (**2005**) Cryogenically cooled probes-a leap in NMR technology, *Progress in Nuclear Magnetic Resonance Spectroscopy 46*, 131-155.

[29] Zhang, R., Mroue, K. H., Ramamoorthy, A. (**2017**) Proton-Based Ultrafast Magic Angle Spinning Solid-State NMR Spectroscopy, *Accounts of Chemical Research 50*, 1105-1113.

[30] Zorin, V. E., Elena, B., Lesage, A., Emsley, L., Hodgkinson, P. (**2007**) On the orientational dependence of resolution in ^{1}H solid-state NMR, and its role in MAS, CRAMPS and delayed-acquisition experiments. *Magnetic Resonance Chemistry 45*, 93-100.

[31] Hore, P. J. ''Nuclear Magnetic Resonance'', p. 9, Oxford University Press, Oxford, **1995**.

[32] Harris, R. K. (**1997**) Nuclear Magnetic Resonance Spectroscopy, a physicochemical view, Longman.

[33] Andrew, E. R., Bradbury, A., Eades, R. G. (**1959**) Removal of dipolar broadening of nuclear magnetic resonance spectra of solids by specimen rotation. *Nature 183*, 1802.

[34] Lowe, I. J. (**1959**) Free induction decay of rotating solids. *Physical Review Letters 2*, 285.

[35] McBrierty V., Packer, K. J. Nuclear Magnetic Resonance in solid Polymers, Cambridge University Press, **1993**.

[36] Ernst, R. R., Bodenhausen, G., Wokuan, A. Principles of Nuclear Magnetic Resonance on One and Two dimensions, Clarendon Press, Oxford, **1987**.

[37] Anderson, W. A., Freeman, R. (**1962**) Influence of a second rf field on high-resolution NMR spectra. *Journal of Chemical Physics 37*, 85-103.

[38] Ernst, M. (**2003**) Heteronuclear spin decoupuling in solid-state NMR under magic-angle sample spinning, *Journal of Magnetic Resonance 110*, 219.

[39] Bennett, A. E., Rienstra, C. M., Auger, M., Lakshmi, K. V., Griffin, R. G. (**1995**) Heteronuclear decoupling in rotating solids. *Journal of Chemical Physics 103*, 6951.

[40] Kono, H., Yunoki, S., Shikano, T., Fujiwara, M., Erata, T., Takai, M. (**2002**) CP/MAS ^{13}C NMR study of cellulose and cellulose derivatives 1. Complete assignment of the CP/MAS ^{13}C NMR spectrum of the native cellulose. *Journal of American Chemical Society 124*, 7506-7511.

[41] Driess, M., Schaller, T., Sebald, A. (**1997**) ^{29}Si CP/MAS NMR of phosphorus-bearing organosilicon compounds. *Solid state nuclear magnetic resonance 2-4*, 219-225.

[42] Reinhard, S., Blümel, (**2003**) ^{31}P CP/MAS NMR of polycrystalline and immobilized phosphines and catalysts with fast sample spinning. *Magnetic Resonance Chemistry 41*, 406-416.

[43] Mehring, M. High Resolution NMR Spectroscopy in Solids, in NMR Basic Principles and Progress, Diehl, P., Kluck, E., Kosfeld, R. (eds.) Springer-Verlag:Berlin, **1976**, 11, Chapter 5.

[44] Metz, G., Ziliox, M., Smith, S. O. (**1996**) Towards quantitative CP-MAS NMR, *Solid State Nuclear Magnetic Resonance 7*, 155-160.

[45] Shu, J., Chen, Q., Zhang, S. (**2008**) Quantification of cross polarization with relaxation compensated reciprocity relation in NMR. *Chemical Physics Letters 462*, 125-128.

[46] Johnson, R. L., Schmidt-Rohr, K. (**2014**) Quantitative solid-state ^{13}C NMR with signal enhancement by multiple cross polarization. *Journal of Magnetic Resonance 239*, 44-49.

[47] Bodenhausen, G., Ruben, D. J. (**1980**) *Chemical Physics Letter 69*, 185-188.

[48] Mansfeld, S. D., Kim, H., Ralph, J. (**2012**) Whole plant cell wall characterization using solution-state 2D NMR. *Nature Protocoll 7*, 1579-1589.

[49] Morris, G. A., Freeman, R. (**1979**) Enhancement of nuclear resonance signals by polarization transfer. *Journal of American Chemical Society 101*, 760-762.

[50] Heikkinen, S., Toikka, M. M., Karhunen, P. T., Kilpeläinen, I. A. (**2003**) Quantitative 2D HSQC (Q-HSQC) via suppression of J-dependence of polarization transfer in NMR spectroscopy: Application to wood lignin. *Journal of American Chemical Society 125*, 4362-4367.

[51] Boyer, R. D., Johnson, R., Krishnamurthy, K. (**2003**) Compensation of refocusing inefficiency with synchronized inversion sweep (CRISIS) in multiplicity-edited HSQC. *Journal of Magnetic Resonance 165*, 253-259.

[52] Zwahlen, C., Legault, P., Vincent, S. J. F., Greenblatt, J., Konrat, R., Kay, L. E. (**1997**) Methods for measurements of intermolecular NOEs by multinuclear NMR spectroscopy: Application to a bacteriophage λ N-peptide/boxB RNA complex. *Journal of American Chemical Society 119*, 6711-6721.

[53] Man, P. P, in ''Encyclopedia of Nuclear Magnetic Resonance'' (D. M. Grant and R. K. Harris, Eds.), Vol. 6, p. 3838, Wiley, Chichester, **1996**.

[54] Samoson, A., Lippmaa, E. (**1983**) Excitation phenomena and line intensities in high-resolution NMR powder spectra of half-integer quadrupolar nuclei. *Physical Reviews B28*, 6567-6570.

[55] Mao, J.-D., Hu, W.-G., Schmidt-Rohr, K., Davies, G., Ghabbour, E. A., Xing, B. (**2000**) Quantitative characterization of humic substances by solid-state 13C NMR. *Soil Science Society American Journal 64*, 873-884.

[56] Pervushin, K., Riek, R., Wider, G., Wütrich, K. (**1997**) Attenuated T2 relaxation by mutual cancellation of dipole-dipole coupling and chemical shift anisotropy indicates an avenue to NMR structures of very large biological macromolecules in solution. *Proceedings of the National Academy of Sciences of the United States of America 94*, 12366-12371.

[57] Overhauser, A. (**1953**) Polarization of Nuclei in Metals. *Physical Review 92*, 411-415.

[58] Freeman, R. (**1997**) A Handbook of Nuclear Magnetic Resonance 2nd ed., Addison Wesley Longman.

[59]Ashbrook, S. E., Dowell, N. G., Prokes, I., Wimperis, S. (**2006**) Nuclear Overhauser Effect (NOE) Enhancement of 11B NMR Spectra of Borane Adducts in the Solid State. *Journal of American Chemical Society 128,* 6782-6783.

[60] Field, L. D., Gardiner, M. G., Messerie, B. A., Raston, C. L. (**1992**) Structure of Dilithio-(*E*)-1,4-bis(trimethylsilyl)but-2-ene by X-ray Crystallography and ^{1}H-^{7}Li HOESY. *Organometallics 11*, 3566-3570.

[61] Berger, S., Müller, F. (**1995**) Locating the Position of Lithium in Solution by Combined ^{13}C, ^{6}Li and ^{1}H, ^{6}Li HOESY Measurements. *Chemische Berichte 128*, 799-802.

[62] Buranov, A. U., Mazza, G. (**2008**) Lignin in straw of herbaceous crops. *Industrial Crops and Products 28*, 237-259.

[63] Brunow, G., Lundquist, K. (**2010**) Functional groups and bonding patterns in lignin (including the lignin-carbohydrate complexes). In Lignin and Lignans: Advances in Chemistry (Heitner, C., Dimmel, D. R., Schmidt, J. A., Eds.) New York: CRC Press, pp. 245-265.

[64] Del Rìo, J., Rencoret, J., Prinsen, P., Martìnez, Á. T., Ralph, J., Gutiérrez, A. (**2012**) Structural characterization of wheat straw lignin as revealed by analytical pyrolysis, 2D-NMR, and reductive cleavage methods. *Journal of Agricultural and Food Chemistry 60*, 5922-5935.

[65] Koshijima, T. Watanabe, T. Association between Lignin and Carbohydrates in Wood and Other Plant Tissues; Springer: Berlin, Germany, **2003**.

[66] Balakshin, M. Y., Capanema, E. A., Gracz, H.; Chang, H.-m. Jameel, H. (**2001**) Quantification of lignin-carbohydrate linkages with high-resolution NMR spectroscopy. *Planta 233*, 1097-1110

[67] Yuan, T.-Q., Xu, S.-N., Sun, R.-C. (**2011**) Characterization of lignin structures and lignin-carbohydrate complexes (LCC) linkages by quantitative ^{13}C and 2D HSQC NMR spectroscopy. *Journal of Agricultural and Food Chemistry 59, 10604-10614.*

[68] Fengel, D., Wegener, G. Wood-Chemistry, ultrastructure, reactions. Walter de Gruyter, Berlin and New York, **1984**, 613 pp.

[69] Sette, M., Lange, H., Crestini, C. (**2013**) Quantitative HSQC analyses of lignin: a practical comparison. *Computational and Structural Biotechnology Journal 6* (7): e201303016.

[70] Rencoret, J., Marques, G., Gutierrez, A.et al. (**2008**) Structural characterization of milled wood lignins from differ-ent eucalypt species. *Holzforschung 62*, 514–526.

[71] del Rıo, J.C., Rencoret, J., Marques, G.et al.(**2008**) Highly acylated (acetylated and/or p-coumaroylated) nativelignins from diverse herbaceous plants. *Journal of Agricultural and Food Chemistry 56,* 9525–9534

[72] Stewart, J.J., Akiyama, T., Chapple, C.et al.(**2009**) The effects on lignin structure of overexpression of ferulate5-hydroxylase in hybrid poplar. *Plant Physiology 150*, 621–635

[73] Akim, L.G., Argyropoulos, D.S., Jouanin, L.et al. (**2001**) Quantitative phosphorus-31 NMR spectroscopy of lignins from transgenic poplars. *Holzforschung 55*, 386–390.

[74] Guerra, A., Filpponen, I., Lucia, L. A., Saquing, C., Baumberger, S., Argyropoulos, D. S. (**2006**) Toward a better understanding of the lignin isolation process from wood. *Journal of Agricultural and Food Chemistry 54*, 5939-5947.

[75] Granata, A., Argyropoulos, D. S. (**1995**) 2-Chloro-4,4,5,5-tetramethyl-1,3,2,-dioxaphospholane, a reagent for the accurate determination of the uncondensed and condensed phenolic moieties in lignins. *Journal of Agricultural Food and Chemistry 43*, 1538-1544.

[76] Faix, O., Argyropoulos, D. S., Robert, D., Neirinck, V. (**1994**) determination of hydroxyl groups in lignins evaluation of ^{1}H-, ^{13}C-, ^{31}P-NMR, FTIR and wet chemical methods. *Holzforschung 48*, 387-394.

[77] Lu, F., Ralph, J. (**2003**) Non-degradative dissolution and acetylation of ball-milled plant cell walls: high-resolution solution-state NMR. *The Plant Journal 35*, 535-544.

[78] Li, S., Lundquist, K. (**2000**) Cleavage of arylglycerol β-aryl ethers under neutral and acid conditions. *Nordic Pulp and Paper Research Journal 15*, 292-299.

[79] Robert, D., Bardet, M., Lapierre, C. (**1988**) Structural changes in aspen lignin during steam explosion treatment. *Cellulose Chemistry and Technology 22*, 221-230.

[80] Nimz, H. (**1966**) A new type of rearrangement in the lignin field. *Angewandte Chemistry 5*, 843.

[81] Li, J., Henriksson, G., Gellerstedt, G. (**2007**) Lignin depolymerization/repolymerization and its critical role for delignification of aspen wood by steam explosion. *Bioresource Technology 98*, 3061-3068.

[82] Yang, Q., Wu, S., Lou, R., Gaojin, L. V. (**2011**) Structural characterization of lignin from wheat straw. *Wood Science and Technology 45*, 419-431.

[83] Fyfe, C. A., Mueller, K. T., Kokotailo, G. T. Solid-state NMR studies of zeolites and related systems; in NMR Techniques in Catalysis (Bell, A., Pines A. Eds.) Marcel Dekker, Inc. **1994**.

[84] Olson, D. H., Haag, W. O. (**1984**) Structure-Selectivity Relationship in xylene isomerization and selective toluene disproportionation. *ACS Symposium Series 284*, 275-307.

[85] Beck, J. S., Dandekar, A. B., Degnan, T. F. (**2002**) in Zeolites for Cleaner Technologies (M. Guisnet and J. P. Gilson, Eds.) Catalytic Science Series, Vol 3, p.223.

[86] Weitkamp, J., in Catalysis and Zeolites: Fundamentals and Applications (Puppe L., Eds.) Springer-Verlag, Berlin, **1999**.

[87] Frising, T., Leflaive, P. (**2008**) Extraframework cation distribution in X and Y faujasite zeolites: A review. *Microporous and mesoporous materials 114*, 27-63.

[88] Remy, M. J., Stanica, D., Poncelet, G., Feijen, E. J. P., Grober, P. J., Martens, J. A., Jacobs, P. A. (**1996**) Dealuminated H-Y zeolites: relation between physicochemical properties and catalytic activity in heptane and decane isomerization. *The Journal of Physical Chemistry B 100*, 12440-12447.

[89] Korkuna, O., Leboda, R., Skubiszewska-Zie'ba, Vrubllevs'ka, T., Gun'ko, V. M., Ryczkowski, J. (**2006**) Structural and physicochemical properties of natural zeolites:clinoptilite and mordenite. *Microporous and Mesoporous Materials 87*, 243-254.

[90] Corma, A., Juan-Rajadell, M. I., López-Nieto, Martinez, A., Martinez, C. (**1994**) A comparative study of O_4^{2-}/ZrO_2 and zeolite beta as catalysts for the isomerization of n-butane and the alkylation of isobutan with 2-butene. *Applied Catalysis A: General 111*, 175-189.

[91] Olson, D. H., Kokotailo, G. T., Lawton, S. L., Meier, W. M. (**1981**) Crystal Structure and structure-related properties of ZSM-5. *The journal of Physical Chemistry 85*, 2238-22413

[92] Blasco, T., Corma, A., Martinez-Triguero, J. (**2006**) Hydrothermal stabilization of ZSM-5 catalytic-cracking additives by phosphorus addition. *Journal of Catalysis 2*, 267-277.

[93] Gierer, J. (**1980**) Chemical aspects of kraft pulping. *Wood Science and Technology 14*, 241-266.

[94] Meier, W. M., Olsen, D. H. Atlas of zeolite structure types. Butterworths: London, **1992**.

[95] Van Laak, A. N. C. Post-Synthesis modifications on zeolites for improved accessibility and catalytic performance. Doctoral Thesis, University of Utrecht, **2011**.

[96] Ek, S., Root, A., Peussa, M., Niinistö, L. (**2001**) Determination of the hydroxyl group content in silica by thermogravimetry and a comparison with ^{1}H MAS NMR results. *Thermocimica Acta 379*: 201-212.

[97] Jiang, Y., Huang, J., Dai, W., Hunger, M. (**2011**) Solid-state nuclear magnetic resonance investigations of the nature, property, and activity of acid sites on solid catalysts. *Solid State Nuclear Magnetic Resonance 39*, 116-141.

[98] Bakhmutov V. I. Solid-Sate NMR in Materials Science: Principles and Applications. CRC Press, **2011**.

[99] Engelhardt, G., Michel, D. In: High resolution solid-state NMR of silicates and zeolites. John Wiley & Sons Ltd, **1987**.

[100] Klinowski, J. (**1991**) Solid-State NMR studies of Molecular Sieve Catalysts. *Chemical Reviews 91*, 1459-1479.

[101] Loewenstein, W. (**1954**) The distribution of aluminium in the tetrahedra of silicates and aluminates. *American Mineralogist 39*, 92-96.

[102] Haase, J., Park K. D., Guo, K., Timken, H. K. C., Oldfield, E. (**1991**) Nuclear Magnetic Resonance Spectroscopic Study of Spin-Lattice Relaxation of Quadrupolar Nuclei in Zeolites. *The Journal of Physical Chemistry C 95*, 6996-7002.

[103] Kennedy, G. J., Afeworki, M., Calabro, D. C., Chase, C. E., Smiley, JR, R. J. (**2004**) 1H MAS NMR (Magic-Angle Spinning nuclear magnetic resonance) techniques for the quantitative determination of hydrogen types in solid catalysts and supports. *Applied spectroscopy 58*, 698-704.

[104] Hunger, M., Ernst, S., Steuernagel, S., Weitkamp, J. (**1996**) High-filed ^{1}H MAS NMR investigations of acidic and non-acidic hydroxyl groups in zeolites H-Beta, H-ZSM-5, H-ZSM-58 and H-MCM-22. *Microporous Materials 6*, 349-353.

[105] Huang, J., van Vegten, N., Jiang, Y., Hunger, M., Baiker, A. (**2010**) increasing the Brönstedt acidity of flame-derived silica/alumina up to zeolite strength. *Angewandte Chemistry International Edition 41*, 7776-7781.

[106] Sjöström, E. (**1993**) Wood Chemistry. Fundamentals and Applications (2nd Ed.). San Diego: Academic Press, Inc. 293 p.

[107] Zhang, Y. P., Lynd, L. R. (**2004**) Toward an aggregated understanding of enzymatic hydrolysis of cellulose: Noncomplexed cellulase systems. *Biotechnology and Bioengineering 88*, 797-824.

[108] Krässig, H. A. (**1993**) Cellulose: Structure, accessibility and reactivity. South Africa: Gordon and Breach Science Publishers. 376 p.

[109] Pinkert, A., Marsh K. N., Pang, S., Staiger M. P. (**2009**) Ionic Liquids and Their Interaction with Cellulose. *Chemical Reviews 109*, 6712-6728.

[110] O'Sullivan, A. C. (**1997**) Cellulose: the structure slowly unravels. *Cellulose 4*, 173-207.

[111] VanderHart, D. L., Atalla, R. H (**1984**) Studies of microstructure in native cellulose using solid-state ^{13}C NMR. *Macromolecules 17*, 1465-1472.

[112] Kuga, S., Takagi, S., Brown, R. M. (**1993**) Native folded-chain cellulose II. *Molecular Polymer 34*, 3293-3297.

[113] Shibazaki, H., Saito, M., Kuga, S., Okano, T. (**1998**) Native cellulose II production by acetobacterial xylinum under physical constraints. *Cellulose 5*, 165-173.

[114] Yamamoto, H., Horii, F. (**1993**) CPMAS carbon-13 NMR analysis of the crystal transformation induced for Valonia cellulose by annealing at high temperatures. *Macromolecules 26*, 1313-1317.

[115] Ye, D. (**2007**) Preparation of nanocellulose. *Prog. Chem. 19*, 1568-1575.

[116] Hubbe, M., Rojas, O., Lucia, L., Sain, M. (**2008**) Cellulosic nanocomposites: a review. *Bioresources 3*, 929-930.

[117] Edgar, K. J., Buchanan, C. M., Debenhamn, J. S., Rundquist, P. A., Seiler, B. D., Shelton, M. C., Tindall, D. (**2001**) Advances in cellulose ester performance and applications. *Progress in Polymer Science 26*, 1605-1688.

[118] Ly, B., Thielemans, B., Dufresne, A., Chaussy, D., Belgacem, M. (**2008**) Surface functionalization of cellulose fibres and their incorporation in renewable polymeric matrices. *Composites Science and Technology 68*, 3193-3201.

[119] Karrasch, A., Jäger, C., Karakawa, M., Nakatsubo, M., Potthast, A., Rosenau, T. (**2009**) Solid-state NMR studies of methyl celluloses. Part 1:regioselectivity substituted celluloses as standards for establishing an NMR data basis. *Cellulose 16*, 129-137.

[120] Sievers, C., Marzialetti, T., Hoskins, T. J. C., Valenzuale Olarte, M. B., Agrawal, P. K., Jones, C. W. (**2009**) Quantitative solid-state NMR analysis of residues from acid hydrolysis of loblolly pine wood. *Bioresource Technology 100*, 4758-4765.

[121] Torri, G., Cosentino, C., Delben, F., Simonutti, R., Sozzani, P. (**1999**) Novel cellulosic ethers with low degrees of substitution-II. Magic angle spinning NMR study. *Carbohydrate Polymers 40*, 125-135.

[122] Jandura, P., Kokta, B. V., Riedl, B. (**2000**) Fibrous long-chain organic acid cellulose esters and their characterization by diffuse reflectance FTIR spectroscopy, solid-state CP/MAS 13C-NMR, and X-ray diffraction. *Journal of Applied Polymer Science 78*, 1354-1365.

[123] Svagan, A., Samir, M., Berglund, L. (**2007**) Biomimetic polysaccharide nanocomposites of high cellulose content and high toughness. *Biomacromolecules 8*, 2556-2563.

[124] Yano, H., Seki, N., Ishida, T. (**2008**) Manufacture of nanofibers and nanofibers manufactures thereby. *Japanese Kokai Tokkyo Koho 17*, 2007-2229.

[125] De Menezes, A. J., Pasquini, D., Curvelo, A. A. D. S., Gandini, A. (**2009**) Self-reinforced composites obtained by the partial oxypropylation of cellulose fibers. 1. Characterization of the materials obtained with different types of fibers. *Carbohydrate Polymers 76*, 437-442.

[126] Matsumura H., Sugiyama, J., Glasser, W. (**2000**) Cellulosic nanocomposites. I Thermally deformable cellulose hexanoates from heterogeneous reaction. *Journal of Applied Polymer Science 78,* 2242-2253.

[127] Tezuka, Y., Tsuchiya, Y., Shiomi, T. (**1996**) ^{13}C NMR determination of substituent distribution in carboxymethyl cellulose by use of its peresterified derivatives. *Carbohydrate Research 291*, 99-108.

[128] GSim – free software tool visualization and processing of experimental and simulated nuclear magnetic resonance (NMR) spectra. https://sourceforge.net/projects/gsim/

[129] (a) Ziegler, K., Holzkamp, E., Breil, H., Martin, H. (**1954**) *Angewandte Chemistry 67*, 541-547; (b) Natta, G. (**1955**) *Macromolecular Chemistry 16*, 213.

[130] Chadwick, J. C., in Fink, G., Mulhaupt, R., Brintzinger, H.-H. (Eds.) (**1995**) Ziegler Catalysts, Springer, Berlin, 427-440.

[131] Albizzati, E., Giannini, U., Morini, G., Smith, C. A., Ziegler, R. C., in: Fink, G., Mulhaupt, R., Brintzinger, H.-H. (Eds.) (**1995**) Ziegler Catalysts, Springer, Berlin, 413-425.

[132] Mason, J. (**1993**) Conventions for the reporting of nuclear magnetic shielding (or shift) tensors suggested by participants in the NATO ARW on NMR shielding constants at the University of Maryland, College Park, July **1992**. *Solid State Nuclear Magnetic Resonance 2,* 285-288.

[133] Haeberlen, U., in Waugh, J. S. (Ed.) Advances in Magnetic Resonance, Academic Press, New York, **1976**.

[134] Paramasivan, S., Balakrishnan, A., Dimitrenko, O., Godert, A., Begley, T. P., Jordan, F., Polenova, T. Solid-State NMR and Density Functional Theory Studies of ionization states of thiamin (**2011**) *Journal of Physical Chemistry B 115*, 730-736.

[135] Mousavi, M., Yu, S.-S.-F., Tzou, D.-L. A (13)C solid-state NMR analysis of vitamin D compounds (**2009**) *Solid state nuclear magnetic resonance 36*, 24-31.

[136] Spiess. H. W., Diehl, P., Fluck, E., Kosfeld, R. (Eds.), NMR Basic Principles and Progress, vol. 15, Springer, Berlin, **1978**.

[137] http://anorganik.uni-tuebingen.de/klaus/nmr/index.php?p=conventions/csa/csa

[138] Peersen, O. B., Wu, X., Kustanovich, I., Smith, S. O. (**1993**) Variable-amplitude cross-polarization MAS NMR. *Journal of Magnetic Resonance 104,* 334-339.

[139] White, J. L., Beck, L.W., Ferguson, D. B., Haw, J. F. (**1992**) Background suppression in MAS NMR. *Journal of Magnetic Resonance 100*, 336-341.

[140] Clayden, N. J., Jones, J. V., J. (**1990**) A study of titanium and magnesium chloride complexes with dialkyl phthalates by solid state 13C CP MAS NMR spectroscopy. *Chemical Society Perkins Transactions 2*, 175-178.